Remote Sensing Applications: Society and Environment 34 (2024) 101151

Contents lists available at ScienceDirect

Remote Sensing Applications: Society and Environment

journal homepage: www.elsevier.com/locate/rsase

Bitou bush detection and mapping using UAV-based multispectral and hyperspectral imagery and artificial intelligence

Narmilan Amarasingam [a,b,c,*], Jane E Kelly [d], Juan Sandino [a,b], Mark Hamilton [e], Felipe Gonzalez [a,b], Remy L Dehaan [d], Lihong Zheng [d], Hillary Cherry [e]

[a] School of Electrical Engineering and Robotics, Faculty of Engineering, Queensland University of Technology (QUT), 2 George Street, Brisbane City, QLD, 4000, Australia
[b] QUT Centre for Robotics, Queensland University of Technology, 2 George Street, Brisbane City, QLD, 4000, Australia
[c] Department of Biosystems Technology, Faculty of Technology, South Eastern University of Sri Lanka, University Park, Oluvil, 32360, Sri Lanka
[d] Gulbali Institute for Agriculture Water and Environment, Charles Sturt University, Boorooma Street, Wagga Wagga, NSW, Australia
[e] NSW Department of Planning and Environment, 12 Darcy Street, Parramatta, 2150, NSW, Australia

ARTICLE INFO

Keywords:
Deep learning
Drone
Machine learning
Remote sensing
Weed identification

ABSTRACT

The use of Unmanned Aerial Vehicles (UAVs) for remote sensing (RS) of vegetation presents a valuable platform for weed monitoring, owing to the high spatial resolution of collected images. Accurate segmentation and mapping of weed spatial distribution plays a pivotal role in achieving effective management and ensures efficient and sustainable utilization of weed control measures. Furthermore, UAV-based RS provides a rapid way of assessing phenological development stages of weed species such as flowering and fruiting. These are often critical stages required for the separation of weed species from surrounding vegetation and are difficult to capture with traditional low resolution airborne and satellite RS imagery. Bitou bush is a shrub and a serious environmental weed of coastal areas of New South Wales (NSW). The primary objective of this study is to develop a model for bitou bush mapping from collected multispectral (MS) and hyperspectral (HS) imagery on location in NSW, Australia by employing various classical machine learning (ML) and deep learning (DL) techniques. The performance of Random forests (RF), Support vector machine (SVM), Extreme gradient boosting (XGB), and K-nearest neighbors (KNN) models is evaluated, achieving overall validation accuracies of 78%, 74%, 80%, and 69%, respectively for bitou bush detection using MS imagery. Subsequently, these models are assessed on HS data, resulting in overall validation accuracies of 77%, 86%, 86%, and 80% for RF, SVM, XGB, and KNN, respectively. Moreover, the DL U-Net model achieved an overall validation accuracy of 92%, outperforming the classical ML models in MS data segmentation tasks. The results of this study highlight the superior performance of the U-Net model in comparison to classical ML models in RS data segmentation, indicating the value of DL techniques for more accurate and robust RS applications such as bitou bush detection and mapping. The insights gained from this research will aid researchers and land managers select appropriate models based on the complexity and characteristics of their RS datasets. Moreover, the integration of UAV RS and artificial intelligence (AI) provide a valuable and efficient platform for bitou bush monitoring and management practices, ultimately enhancing the efficiency and sustainability of weed control efforts.

* Corresponding author. School of Electrical Engineering and Robotics, Faculty of Engineering, Queensland University of Technology (QUT), 2 George Street, Brisbane City, QLD, 4000, Australia.
E-mail addresses: narmilan.amarasingam@hdr.qut.edu.au, narmilan@seu.ac.lk (N. Amarasingam).

https://doi.org/10.1016/j.rsase.2024.101151
Received 11 September 2023; Received in revised form 30 January 2024; Accepted 30 January 2024
Available online 9 February 2024

1. Introduction

Monitoring changes in biodiversity, health, and vegetation cover, is becoming increasingly important to land managers, who consider it a top priority worldwide (Yang and Everitt, 2010). Currently, the protection of natural habitats and biodiversity faces significant challenges from invasive weed species (Harun et al., 2014). These non-native plant species spread rapidly and aggressively, covering extensive areas, and causing detrimental effects on native species and their habitats (Harun et al., 2014; Papp et al., 2021). Therefore, weed detection and mapping remains an essential initial step in weed control (Hu et al., 2021; Khaliq et al., 2019; Reedha et al., 2022). Traditional methods of weed surveillance, such as on-ground assessments, are costly and time-consuming, and alternative techniques are needed to ensure effective control. Weed detection can be performed by remote sensing (RS) techniques which serve as a key tool for monitoring vegetation (Khaliq et al., 2019; Razfar et al., 2022; Wijesingha et al., 2021). RS provides comprehensive data coverage across different spatial, spectral, and temporal resolutions. UAV based RS and machine learning (ML) algorithms can enhance the sustainability of weed management by precisely detecting weeds in different landscapes (Roslim et al., 2021). Autonomous detection techniques that use UAV derived multispectral (MS) imagery and hyperspectral (HS) imagery have demonstrated highly encouraging outcomes for weed identification in diverse areas (Razfar et al., 2022). Nevertheless, the effective automated identification of weeds in remotely sensed images by ML can be challenging due to similarities in spectral, textural, and shape characteristics of the vegetation (Alexandridis et al., 2017).

Bitou bush (*Chrysanthemoides monilifera* ssp. *rotundata*), a native species of coastal South Africa, has spread to eastern Australia (Lindsay and French, 2006), where it has taken over large areas of the coastline, particularly in New South Wales (Lindsay and French, 2005). It is a perennial shrub that grows up to 5 m tall and has yellow flowers. The leaves are bright lime green, smooth, oval to oblong in shape, and about 3–7 cm long. The flowers are bright yellow and about 2–3 cm in diameter (Department of Agriculture and Fisheries, 2020). Bitou bush seeds spread rapidly via ingestion by birds. It is considered one of the worst weeds in Australia, due to its invasiveness and negative economic and environmental impacts (Department of Agriculture and Fisheries, 2020). It restricts the establishment of various native plant species, possibly due to its allelopathic effects (Ens et al., 2009). Precise detection and mapping of bitou bush are the first step towards implementing effective control.

RS of weeds is gaining significant research interest due to the rapid development of advanced sensors, the emergence of easily accessible and flexible moving platforms (such as UAVs) and recent advancements in artificial intelligence (AI) (Su et al., 2022). Due to the increasing affordability of UAVs, along with the improved capabilities of the sensors they carry (Di Gennaro et al., 2022), these aerial devices are now widely used for acquiring accurate aerial images (Narmilan et al., 2022a, 2022b). These images are applied to effectively map, characterize, and manage environmental landscapes (Hamylton et al., 2020). The use of UAVs has also garnered increasing interest in recent years for tasks such as vegetation monitoring, vegetation mapping, and precision agriculture (de Camargo et al., 2021; Lu et al., 2020) and they have received considerable attention as a valuable tool for weed localisation and management (Chang et al., 2020; Dian Bah et al., 2018; Xia et al., 2022). UAVs provide a promising alternative to conventional aircraft in terms of flexible timing and the ability to fly at extremely low altitudes, allowing them to capture imagery with exceptionally high spatial resolution (Sa et al., 2018). However, despite notable advancements in UAV acquisition systems, automatic weed detection remains a challenging task due to the inherent resemblance between weeds and non-target plants (Dian Bah et al., 2018).

1.1. Related works

A UAV equipped with RGB, MS, and HS sensors enables the precise and effective detection and identification of weeds (Etienne and Saraswat, 2019). Nevertheless, there is a restriction on the number of sensors that can be mounted on a UAV, making the selection of the best combination of spectral bands intricate, yet crucial, for conventional imaging systems using UAVs (Ishida et al., 2018). In certain situations, the application of MS images is beneficial as they possess distinct bands, including red edge or near infrared (NIR) bands (Narmilan et al., 2022b). This enables the differentiation of plants, even when they exhibit similarities in the visible spectrum (Red, Green, Blue) and in leaf shape (Dian Bah et al., 2018). However, HS imaging has seen significant advancements, offering the potential to improve weed detection accuracy and differentiate more clearly between like weed species (Roslim et al., 2021). Adopting HS sensors provides an opportunity to enhance the accuracy of weed detection and species discrimination (Martín et al., 2023). Most studies have focused on using RGB or MS cameras with limited spectral bands, posing challenges in distinguishing between crops and similar weed species. There have been less studies focused on comparing MS with HS imagery for effective weed detection. Therefore, this study was undertaken to compare the use of both MS and HS imagery for the detection of bitou bush in an Australian mixed landscape.

In RS, AI is one of the classification techniques that involves categorizing imagery based on reflected light from Earth's surface (Osorio et al., 2020). When combined with UAVs, this offers efficient weed detection with minimal human involvement (Haq, 2021; Razfar et al., 2022). Deep Learning (DL) based systems for crop and weed identification reduce costs and minimise environmental impact, but accuracy limitations in recent years have been apparent, attributed to factors such as wavelength selection, spatial resolution, and hyperparameter tuning (Haq, 2021). Recently, DL models (MobileNetV2, ResNet50, and SegNet) have demonstrated remarkable outcomes in various intricate classification tasks (Sa et al., 2018; Xia et al., 2022; Razfar et al., 2022). This approach demands a considerable quantity of training data and generating extensive agricultural datasets with expert-level pixel annotations (labelling) is an exceedingly time-consuming endeavour (Dian Bah et al., 2018). In recent years, increased effort has been focussed on developing automatic labelling techniques with DL models to create efficiencies in workflows, with several studies using vegetation indices and achieving precision values between 69% and 93% (Dian Bah et al., 2018). Other studies report the superiority of automatic labelling techniques over manual labelling, improving overall accuracy by 8% (Huang et al., 2015). Table 1 provides a summary of research studies focussed on weed detection using UAV imagery and classical ML and DL techniques.

Table 1
Previous studies using UAV-acquired RGB, multispectral and hyperspectral imagery and artificial intelligence for detection of weeds in various landscapes.

Weeds/fields	Imagery	ML Model/s	Accuracy	References
Bitou bush	RGB	MLPR	82%	Hamylton et al. (2020)
Bitou bush	RGB	ANN	88%–97%	Harris et al. (2017)
Milk thistle weed	MS	SVM	96%	Alexandridis et al. (2017)
Amaranth, Pigweed, and Mallow weed	MS and HS	NN and OBIA	92%	Che'ya et al. (2021)
Parthenium Weed	RGB and HS	YOLOv4 and XGB	86%–99%	Costello et al. (2022)
Weeds in rice field	RGB	mageNet	77.5%	Huang et al. (2018)
Weeds in sugar beet fields	MS	WeedNet, DeepLabv3+, and Gated-SCNN	F_1 score: 85.6–99%	Khoshboresh-Masouleh and Akhoondzadeh (2021)
Yellow bristle, wind grass giant buttercup, and Californian thistle	HS	PLSD, SVM, and MLP	70%–100%.	Li et al. (2021)
Johnsongrass	HS	SAM and SMA	60%–80%	Martín et al. (2023)
Weeds in lettuce field	MS	SVM, YOLOv3, and Mask R–CNN	F1-scores: 88%, to 94%	Osorio et al. (2020)
Common milkweed	HS	SVM and ANN	92.95%–99.61%	Papp et al. (2021)
Weeds in a soybean field	RGB	MobileNetV2, ResNet50, and custom CNN	97.7%	Razfar et al. (2022)
Weeds in sugar beet fields	RGB and MS	SegNet	57.6%–86.3%	Sa et al. (2018)
blackgrass weed	MS	RF	93%	Su et al. (2022)
barnyard grass and velvetleaf	RGB and MS	DCNN	81.1%–92.4%	Xia et al. (2022)

ANN: Artificial Neural Network, MLPR: Maximum Likelihood Parametric Rules, NN: Nearest Neighbor, OBIA: Object Based Image Analysis, PLSD: Partial least squares-discriminant analysis, SVM: Support Vector Machine, MLP: Multilayer Perceptron, SAM: Spectral Angle Mapper, SMA: Spectral Mixture Analysis, DCNN: Deep Convolutional Neural Network.

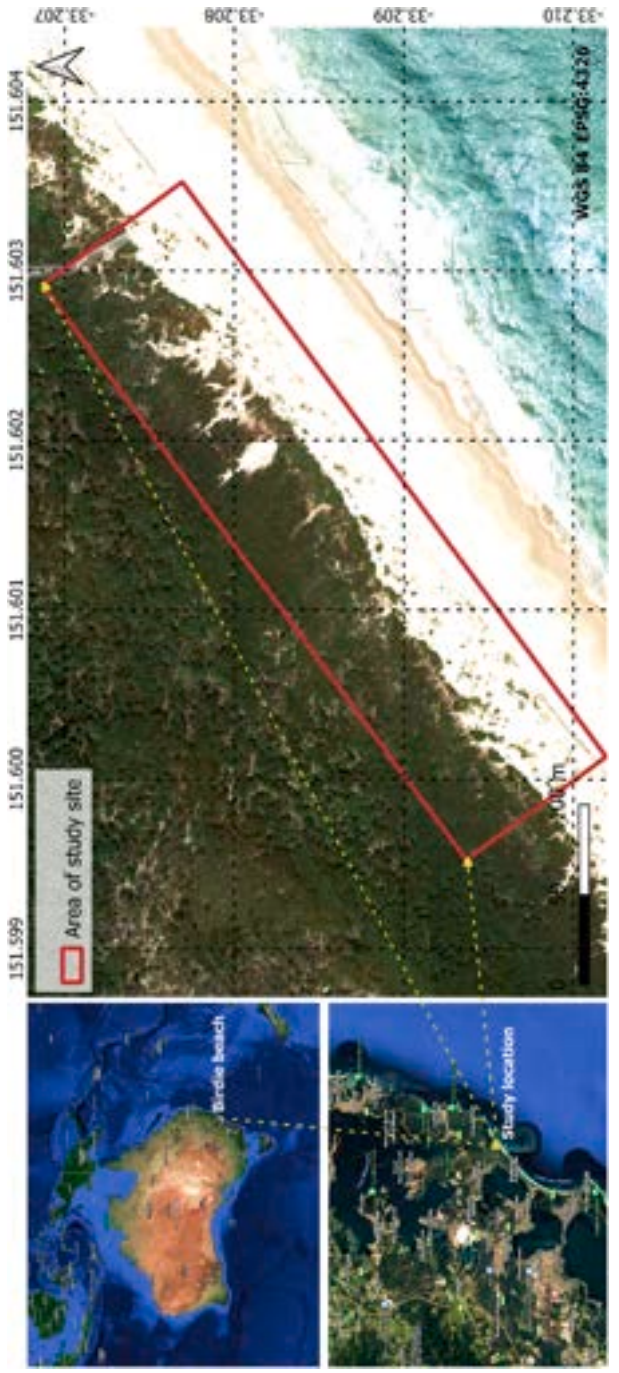

Fig. 1. Study site at Birdie beach, NSW, Australia.

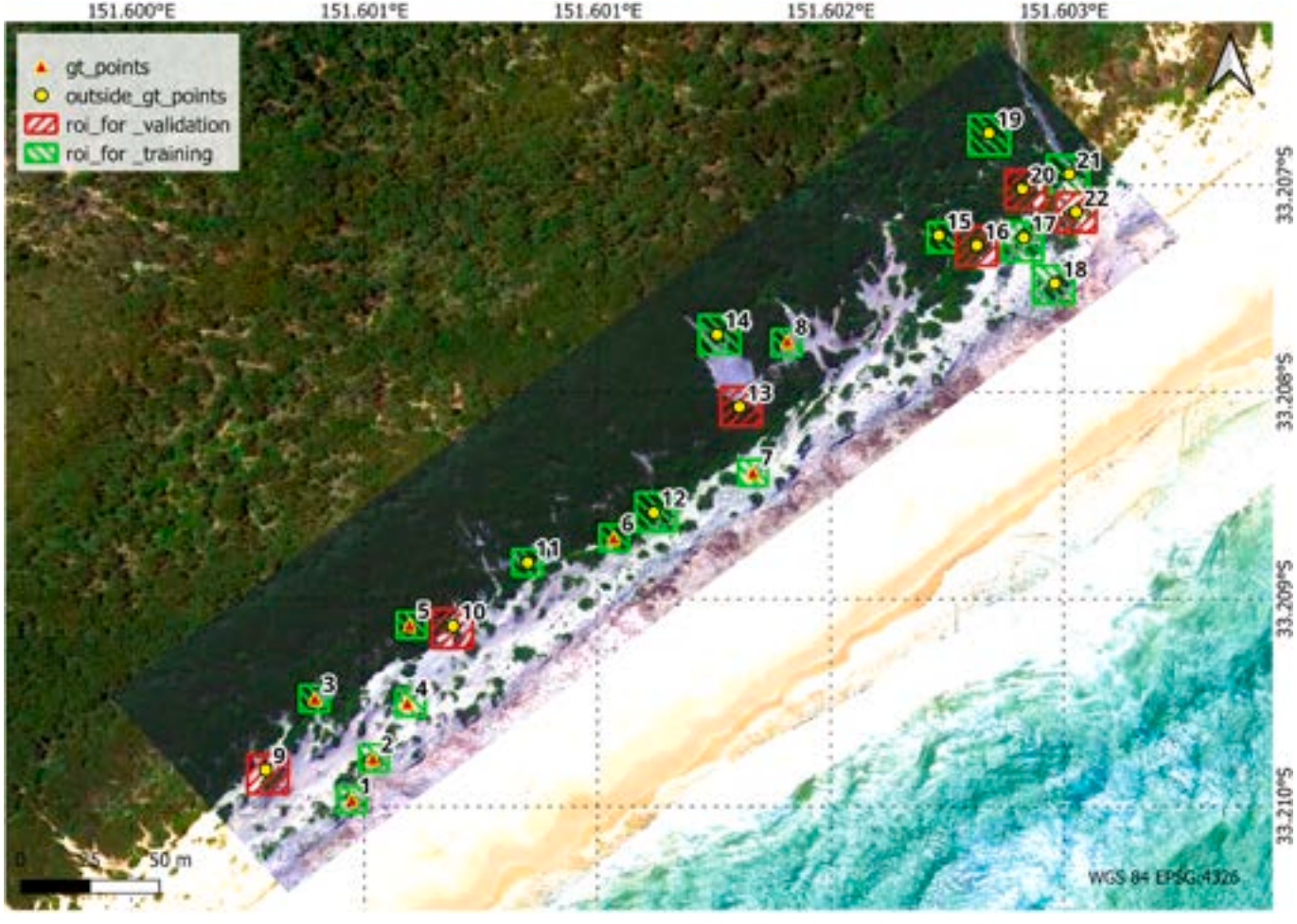

Fig. 2. Geolocations of plots from ID 1 to ID 22 within the study site, with 16 plots allocated for training and the remaining 6 plots designated for validation.

Table 2
Overview of geospatial and vegetation data collected for each plot (ID 1 to 8) within the study site.

ID	Latitude	Longitude	Altitude	Percentage of bitou bush	Average height of bitou bush (cm)	Percentage of other species
1	−33.2095790	151.6004870	12.590	60	45	40
2	−33.2094150	151.6005710	13.680	1	100	99
3	−33.2091820	151.6003110	16.620	65	70	35
4	−33.2091950	151.6007050	13.980	75	25	25
5	−33.2089190	151.6006930	16.570	20	100	80
6	−33.2085830	151.6015220	12.580	75	140	25
7	−33.2083430	151.6019630	11.910	30	15	70
8	−33.2078090	151.6021400	18.410	45	110	55

1.2. Research focus and objectives

Significant progress in weed detection has occurred using UAV imagery and ML or DL techniques. However, there are still notable research gaps where landscape complexity and species diversity in heterogeneous landscapes present much greater challenges for detection than homogenous crop settings. Furthermore, questions remain regarding the comparative value of MS versus HS imagery for detecting weed species in these landscapes, as well as the effectiveness of manual labelling during model development. To address these research gaps, this study sought to use UAVs equipped with MS and HS sensors and ML techniques (with manual labelling) to detect bitou bush at Birdies beach, on the central coast of New South Wales (NSW),Australia. The three specific objectives of this project are to: (1) compare the performance from four clasical ML models (i.e., Random forests (RF), Support vector machine (SVM), Extreme gradient boosting (XGB), and K-nearest neighbors (KNN)) and one DL model (U-Net) to segment bitou bush using UAV MS imagery; (2) evaluate the weed segmentation performance achieved by the ML models using UAV HS imagery; and (3) validate the use of semi-automatic data labelling as a solution for mitigating the cost and labour burden of manual image labelling in weed segmentation and mapping.

2. Materials and methods

2.1. Study site

The UAV MS and HS imaging data used in this research was acquired at Birdies beach, NSW, Australia, during May 2022 as shown in Fig. 1. The imagery covers an area of interest of 4.5 ha, which contains bitou bush at variable densities.

2.2. Ground referencing

Distinctive striped tape was randomly placed along the study site to demarcate eight plots, each identified from ID 1 to 8 as shown in Fig. 2. The geolocation of each plot was precisely recorded for labelling processes. Subsequently, in collaboration with a weed expert, visits were conducted to each plot in the site for the comprehensive collection of information. This included obtaining the percentage of the target species density (bitou bush) and recording its height. The percentages of other species densities were also documented and are presented in Table 2. Accurate ground photos were taken of the plots and all plant species identified. To enhance the number of datasets for ML model training, additional plots beyond the initial eight were incorporated. Specifically, these plots numbered from ID 9 to 22 were randomly drawn in the geotagged MS orthomosaic as shown in Fig. 2. This expansion aimed to provide a more extensive and diverse set of samples for robust ML model training. The identification of the target species within these additional plots (ID 9 to 22) was carried out in collaboration with a weed expert. This involved a thorough examination and labeling of the species present in the MS orthomosaic. The inclusion of these supplementary plots not only increases the overall dataset size but also contributes to the richness and variety of the training samples, ensuring the ML model is well-equipped to handle a broader range of scenarios and variations. Fig. 3 shows the sample images of plots delineated with distinctive striped tapes, encompassing both bitou bush and visually similar species. Weather conditions played a crucial role in the UAV data collection process. Therefore, parameters such as cloud cover, wind speed, humidity, and temperature were systematically recorded and are detailed in Table 3 during data collection in the study site.

2.3. Aerial data collection

UAV flights were conducted utilizing a MicaSense Altum (AgEagle Aerial Systems Inc, Wichita, Kansas, United States of America)

Fig. 3. A sample of images showing ground plots marked with distinctive striped tapes. Plots included bitou bush and similar looking species: (a) plot ID 1, (b) plot ID 3, (c) plot ID 2, (d) plot ID 8.

Table 3
Meteorological parameters and readings during UAV data collection.

Parameters	Reading
Humidity	51 %
Wind speed	3.62 ms^{-1}
Temperature	24 °C
Cloud cover	0–15 %

mounted on a DJI Matrice 300, (Da-Jiang Innovations (DJI), Shenzhen, Guangdong, China) and Specim AFX VNIR (Specim, Spectral Imaging Ltd, Oulu, Finland) was mounted on a DJI M600 (Fig. 4). The MicaSense Altum featured MS capabilities with five bands, including red, green, blue, red edge, and NIR. The Specim AFX VNIR, covering the electromagnetic spectrum from 400 to 1000 nm with 448 bands, offered HS data. The flights were back-to-back with each camera mounted on a different UAV so as to minimise time delay and changes in sunlight conditions between each camera. The flights were parallel to the beach across the foredune where the weeds were growing in high densities as shown in Fig. 5. The flights took place between 10:00 and 13:30 local time in sunny conditions. The MS data was flown at 50m (AGL) with a front and side overlap of 75% resulting in a ground sampling distance (GSD) of 2.2cm/pixels. The HS imagery was flown as a single line at 50m above ground level (AGL) resulting in a 3.5cm/pixel GSD and 34m swath. HS data was collected at a rate of 200Hz exposure with utilizing a field of view (FOV) of 38° and a flight speed of 5 m/s. The AFX camera employed Real-Time Kinematic Global Navigation Satellite System (RTK GNSS) technology, along with a high-end inertial measurement unit (IMU) for reconstructing the image and to allow for georeferencing.

2.4. Image pre-processing

2.4.1. Orthomosaic generation

The raw MS images were converted to reflectance using in-field reflectance panels and Agisoft Metashape 1.6.6 (Agisoft LLC, Petersburg, Russia) to create georeferenced point clouds, digital elevation models, reflectance images and orthomosaics. The raw HS data (data cubes) were radiometrically calibrated from raw digital number to radiance using SPECIM Caligeo Pro and onboard calibration files were acquired at the time of image capture. Radiance images were then converted to reflectance using DROACOR physical atmospheric correction optimized for reflectance and then georeferenced using RTK GPS data to match the image information with specific locations on the earth.

2.4.2. Georeferencing

The methodology applied encompasses the manual georeferencing of HS orthomosaic by referencing it to a MS orthomosaic using QGIS 3.2.0 (Open-Source, Geospatial Foundation, Chicago, IL, USA) software. This process entailed configuring linear transformation parameter and employing cubic resampling. For precise spatial alignment, 20 Ground Control Points (GCPs) were strategically marked across both MS and HS orthomosaics. GCPs were marked by using the ground control panels placed in a randomized manner to cover the entire study area. This georeferencing technique is crucial for identifying different classes in the low-resolution HS orthomosaic. Therefore, labelled pixels from MS imagery were used as a reference to label HS imagery, and subsequently to develop the detection models as explained in Sections 2.5 and 2.6.

2.4.3. Extraction of region of interest

Regions of Interest (ROIs) were extracted from 22 plots (as outlined in Section 2.2), using QGIS software, each measuring 1024 x 1024 pixels. Of these, 16 ROIs were allocated for training and testing (75% of the total), and 6 ROIs were reserved for validation (25% of the total), as depicted in Fig. 2. For the DL U-Net model, image patches of 256 x 256 pixels were utilized, with 256 patches used for training and testing (75% of the total) and 96 patches used for validation (25% of the total). The validation ROIs were employed solely for verifying the classification performance of the model and were not used during the training process. Employing multiple ROIs in place of the complete orthomosaic confers distinct advantages, such as the significant reduction in computational complexity. This, approach allows ML algorithms to focus on localized data for alignment. Table 4 shows the overview of input dataset used for training the different ML models. Fig. 6 displays the ROIs designated for training, testing and validation in the study.

2.5. Image labelling

In ML, labeling involves annotating or categorizing data to facilitate model training. The two labeling approaches encompassing semi-automatic labeling and manual labeling were used in this study. QGIS 3.2.0 software was employed for both labeling techniques

Fig. 4. (a) MicaSense Altum mounted on DJI Matrice 300, (b) Specim AFX VNIR mounted on DJI M600.

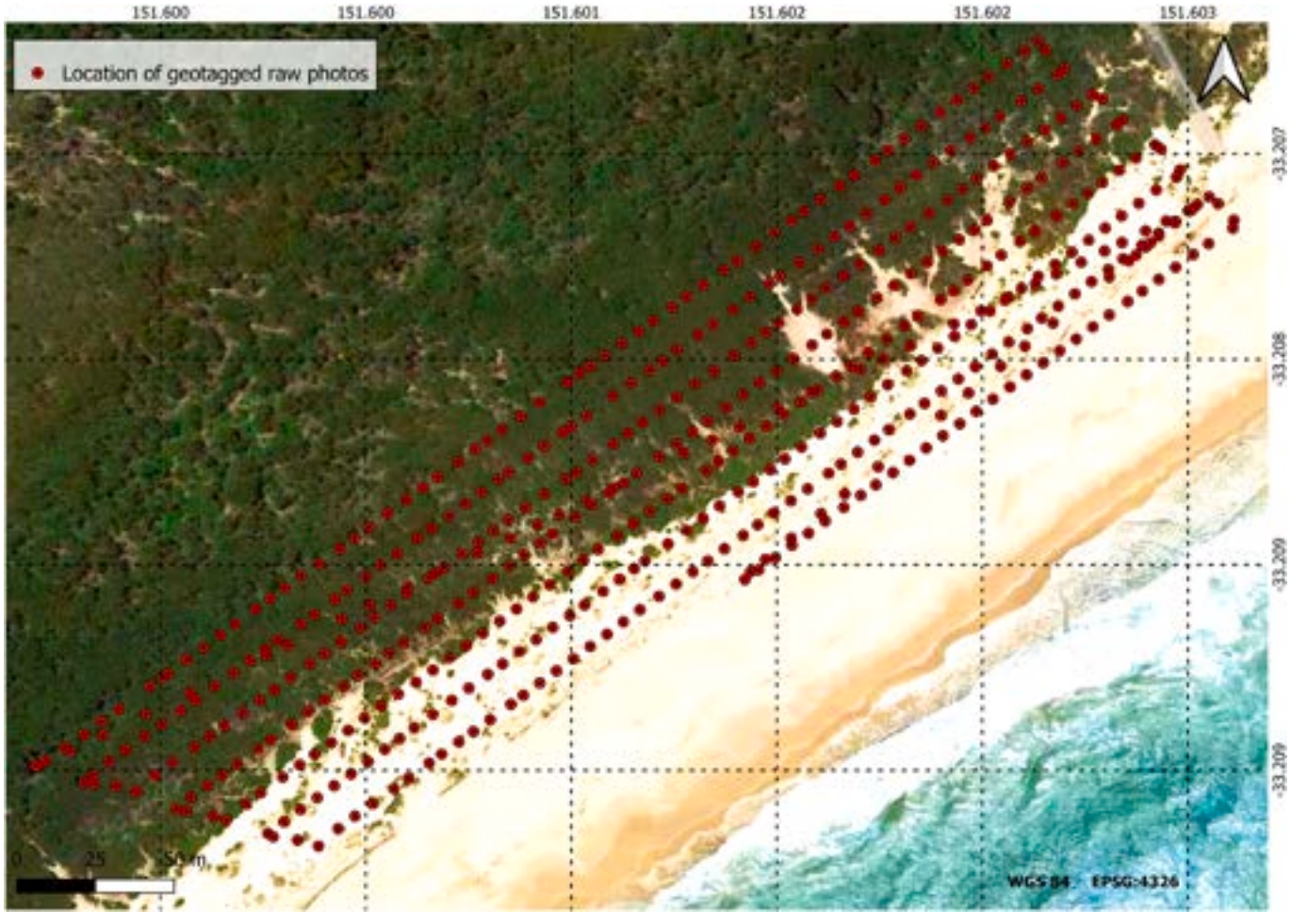

Fig. 5. Flight plan of the MicaSense Altum mounted on DJI Matrice 300, with the flight path overlaid on Google Earth satellite imagery.

Table 4
Overview of dataset used in this study.

Dataset	Frequency	Description
Multispectral raw images	3012	MicaSense Altum mounted on M600 was used
Orthomosaic	1	Agisoft Metashape 1.6.6 was used
Regions of Interest (ROIs)	22	Extraction of ROIs (1024 x 1024) was performed by utilizing polygons from the 22 plots as detailed in Section 2.2.
ROIs for training and testing	16	Around 75% of ROIs were used as shown in Fig. 2.
ROIs for validation	6	Around 25% of ROIs were used as shown in Fig. 2.
Image patches for training	192	Image patches (tile of 256 x 256) from 16 ROIs were used for the DL U-Net model as detailed in Section 2.6.2. The "train_test_split" function from scikit-learn was used to randomly split the image patches for training (75%) and testing (25%).
Image patches for testing	64	
Image patches for validation	96	Around 25% of image patches (tile of 256 x 256) from 6 ROIs were used for the DL U-Net model as detailed in Section 2.6.2.

over MS and HS ROIs.

2.5.1. Manual labelling

The manual labeling was conducted by utilizing plot information (Table 2) from ID 1 to 8 and the remaining plots from ID 9 to 22, assisted by a weed expert. Geolocated ground truth points (Fig. 2) were overlaid on MS ROIs, and pixelwise labeling was executed with precision. Integer values were assigned to each pixel, representing three classes: Id = 1 for bitou bush, Id = 2 for other vegetation, and Id = 3 for non-vegetation. Pixelwise labeling within each ROI was performed with 100% confidence with the expert's support. Unlabeled pixels were designated as Id = 0. Subsequently, the labelled vectors were converted into a rasterized mask using Python code and 22 rasterized labelled masks were obtained for respective MS ROIs. Finally, each rasterized mask portrayed four classes: Id = 0 for unlabeled, Id = 1 for bitou bush, Id = 2 for other vegetation, and Id = 3 for non-vegetation. To avoid mixed pixels of two classes, margins of particular classes were intentionally left unlabeled, implying that the center part of classes was labelled. This pixelwise classification relied solely on spectral information. During classical ML model development, Id = 0 pixels were ignored by masking the ID = 0 from rasterized mask ROIs, and only labelled pixels were considered for model training. For the DL U-Net model, the loss function employed was categorical cross-entropy, with a specific parameter setting of ignore_class = 0, designed to exclude class Id = 0 during model training. Fig. 7 visually illustrates the labelled classes, with unlabeled areas represented in black, and bitou bush, other vegetation, and non-vegetation presented in red, green, and blue, respectively. Fig. 8 illustrates the processing pipeline for bitou bush detection through manual labeling.

2.5.2. Semi-automatic labelling

The semi-automatic labelling technique was subsequently introduced to label the MS imagery more efficiently during the labelling process. Therefore, different vegetation indices (VIs) (as shown in Table 5), including Normalized Difference Vegetation Index (NDVI), Excess Green (ExG), and Leaf Chlorophyll Index (LCI) were used to develop the mask layers. Table 6 presents the threshold values for key VIs, outlining the minimum and maximum spectral values associated with distinct vegetation classes. NDVI values between 0.4632 and 0.5974 characterize areas dominated by bitou bush. ExG values falling within the range of −0.4 to 0.2 identify non-vegetated areas. Additionally, LCI values spanning from 0.4877 to 0.7439 signify regions containing other types of vegetation. These defined threshold ranges assist in the classification and separation of specific vegetation classes in the study area.

Fig. 9 showcases various VIs, including a MS ROI, NDVI, ExG, and LCI, providing a comprehensive visual representation of key spectral characteristics. Fig. 10 provides a visual representation of a MS ROI, masked bitou bush using NDVI, masked non-vegetation using ExG and masked other vegetation using LCI based on threshold values. Fig. 11 presents the (a) ROI of MS imagery and (b) semi-automatic labelled ROI achieved through thresholding techniques. Bitou bush is highlighted in red, other vegetations in green, and non-vegetations in blue for clear visual differentiation. Fig. 12 shows the processing pipeline for semi-automatic labelling of MS imagery.

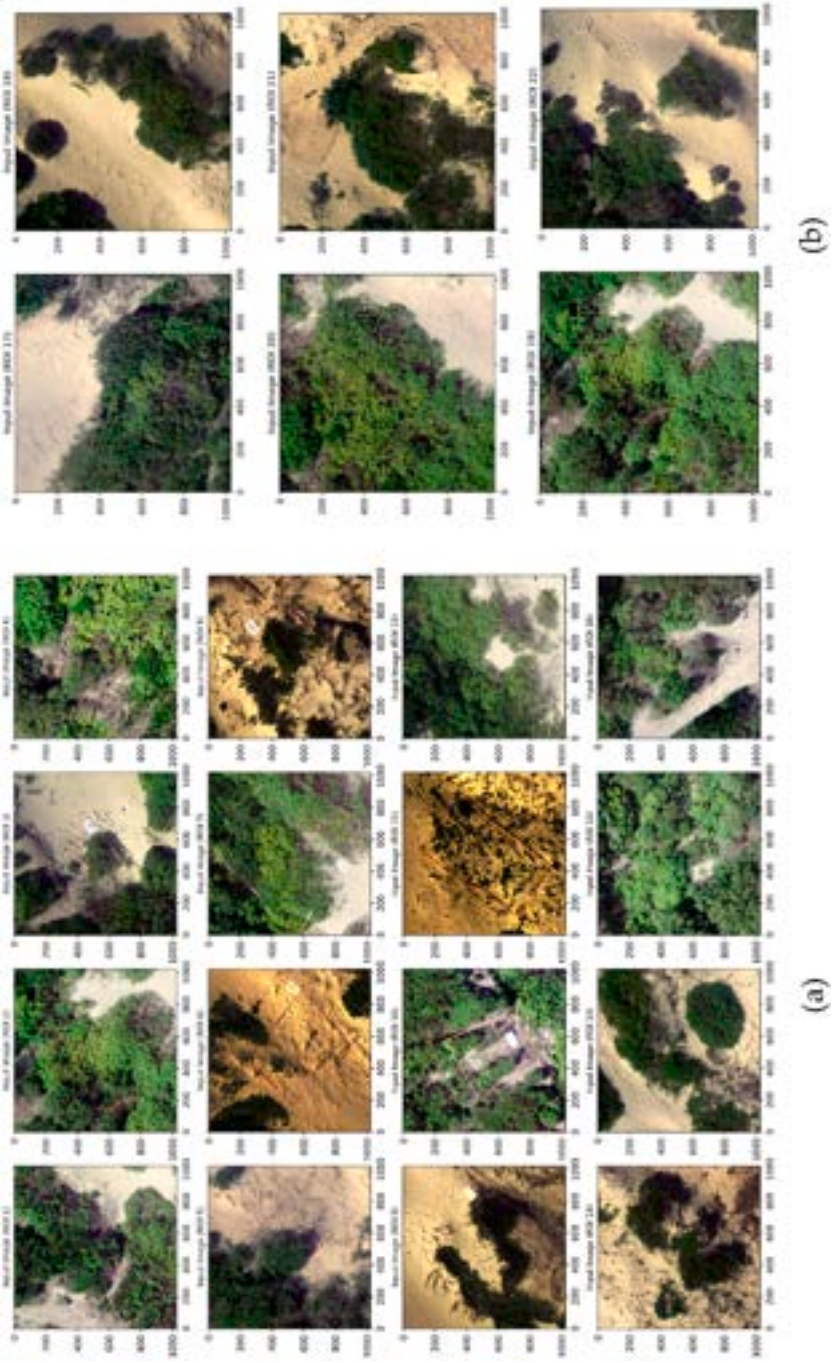

Fig. 6. (a) Region of interests (ROIs) for training and testing (b) ROIs for model validation.

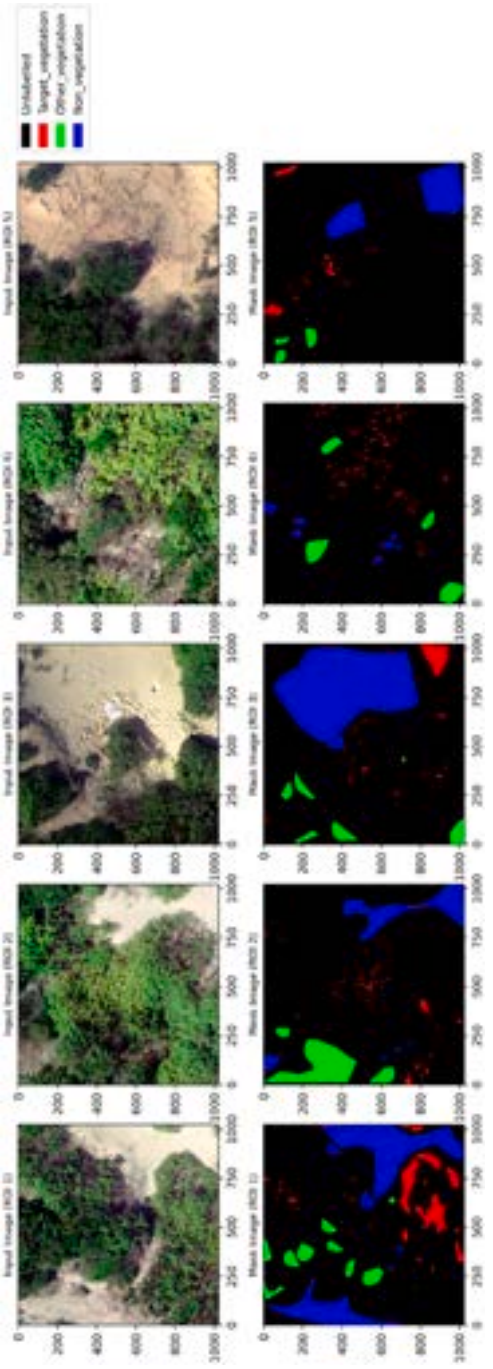

Fig. 7. Labelled masks for different ground truth locations.

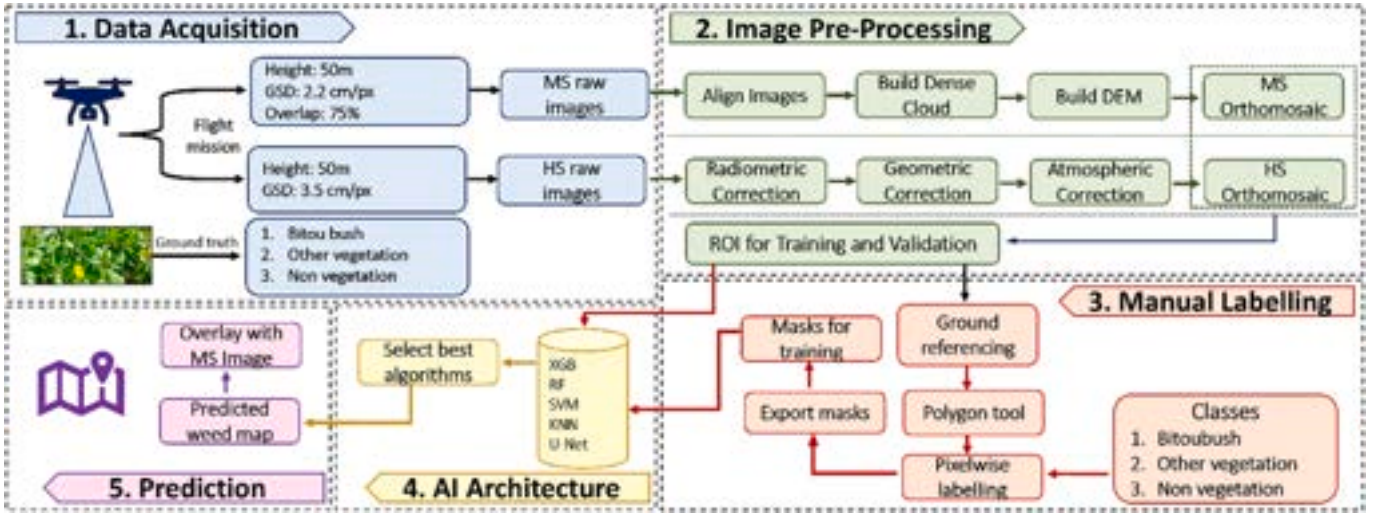

Fig. 8. Processing pipeline for bitou bush detection using manual labelling.

Table 5
Vegetation indices used in this study.

Vegetation indices	Formula	References
NDVI	$NDVI = \frac{NIR - R}{NIR + R}$	Imran et al. (2020)
ExG	$ExG = \frac{2G - R - B}{R + G + B}$	Kerkech et al. (2018)
LCI	$LCI = \frac{NIR - Red\ Edge}{NIR + R}$	Yu et al. (2021)

Normalized Difference Vegetation Index (NDVI), Excess Green (ExG), Leaf Chlorophyll Index (LCI), Red(R), Green (G), Blue (B), Near Infra-red (NIR).

Table 6
Threshold values for vegetation indices and corresponding separated classes.

Vegetation indices	Minimum threshold spectral value	Maximum threshold spectral value	Separated class
NDVI	0.4632	0.5974	Bitou Bush
ExG	−0.4	0.2	Non-vegetations
LCI	0.4877	0.7439	Other vegetations

2.6. Model training for bitou bush mapping

This study conducted a comparative analysis between classical ML models including SVM, RF, KNN, and XGB, as well as the DL model U-Net. The aim was to assess the performance and effectiveness of these models. Output from manual labeling technique was trained to develop all the models mentioned above but the output from the semi-automatic labeling technique was trained to develop the XGB only for this study. SVM is a versatile ML model used for classification and regression analysis (Kumar Nagothu et al., 2023), while RF is another ML model that combines multiple decision trees through majority voting, resulting in robust and accurate predictions (Kumar Nagothu et al., 2023; Dian Bah et al., 2018). In addition, XGB is a type of ensemble ML method used for predictive modelling in classification tasks, while KNN is a non-parametric ML algorithm used for both classification tasks (Vaishnnave et al., 2019). In contrast, DL models, like U-Net, use neural networks with multiple layers to automatically learn hierarchical representations from raw data but require large amounts of labelled data for training and are specifically designed for image segmentation tasks. The popularity of employing the U-Net model for weed detection has grown significantly, primarily attributed to its exceptional precision in distinguishing weeds from crops in images (Yu et al., 2022; He et al., 2022).

Numerous processes are involved in constructing models, including loading, pre-processing, fitting the classifier to the data, and prediction. The processing phase transforms the read input into a set of features, which the classifier subsequently analyses. Several python libraries were utilized for data processing and ML, including Geospatial Data Abstraction Library (GDAL) 3.0.2, XGBoost 1.5.0, Scikit-learn 0.24.2, OpenCV 4.6.0.66, and Matplotlib 3.0. During MS processing, different regions of the MS images with five reflectance bands were smoothed using a low pass filter in ENVI 5.5.1 (Environment for Visualizing Imagery, 2018, L3Harris Geospatial Solutions Inc, Broomfield, Colorado, United States) to decrease the disparity between pixel values by averaging nearby pixels. This was done to improve accuracy in detection before the images were imported into the algorithm. The reflectance bands at wavelengths of 475.0 nm, 560.0 nm, 668.0 nm, 717.0 nm, and 842.0 nm (corresponding to blue, green, red, red edge, and near infrared regions) were loaded into the different models.

The study used an HS image with 448 bands, but only a subset of carefully selected bands was employed in the ML for identification of bitou bush. After manual labelling of HS ROI as explained in section 2.5, labelled regions of the HS ROI were used to separate important spectral bands that showcased discernible variations among classes using standard deviation. The process involved computing absolute differences in spectral values across an array of wavelengths. Initially selecting the top 50, then 100, and ultimately 150 bands with the most pronounced discrepancies from each class pair, the approach was refine based on ML performance. Bands that appeared more than once were removed to prevent repetition between class pairs, resulting in a final streamlined set of 175 unique bands. These chosen bands were crucial in creating a custom ML model designed for detecting Bitou bush, covering a range from 481.17 nm to 773.54 nm. Fig. 13 provides a graphical representation of spectral signature curves, highlighting regions associated with these selected bands. This methodology yielded a diverse range of benefits, encompassing noise reduction, interpretability

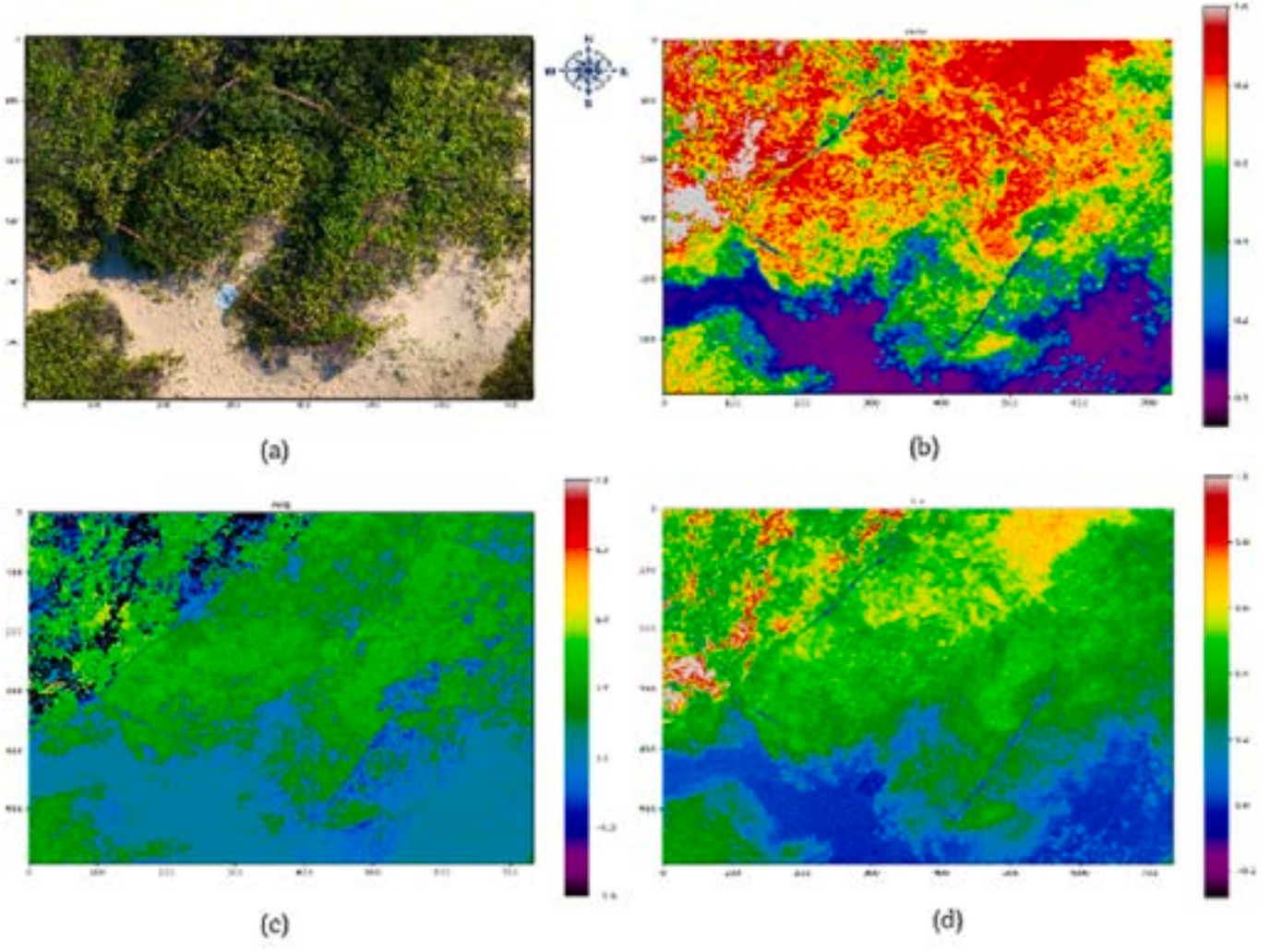

Fig. 9. (a) Multispectral ROI; (b) normalized difference vegetation Index (NDVI); (c) excess green (ExG); and (d) leaf chlorophyll Index (LCI). (For interpretation of the references to colour in this figure legend, the reader is referred to the Web version of this article.)

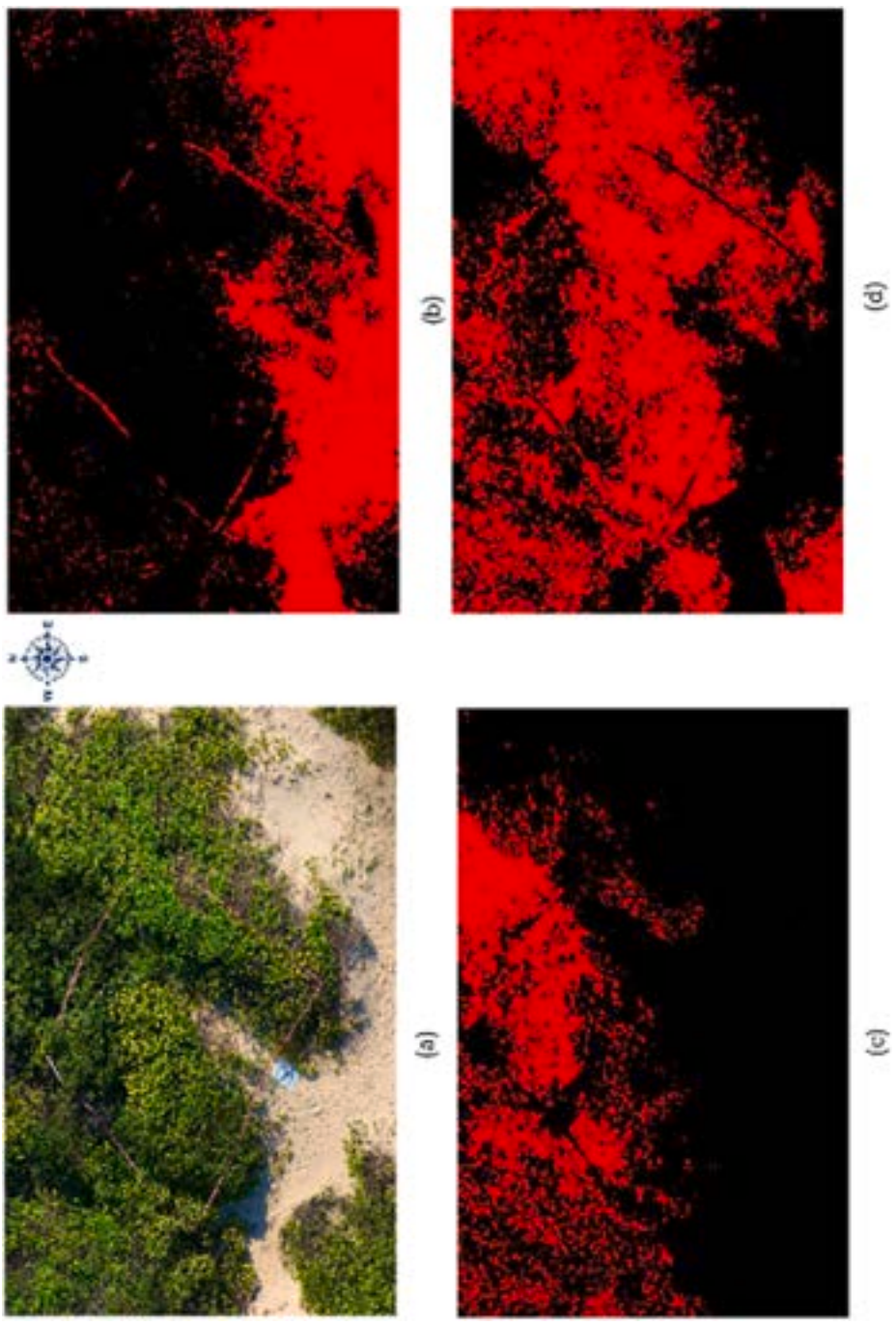

Fig. 10. (a) Multispectral ROI; (b) Masking of Non vegetation; (c) Masking of Other vegetation; and (d) Masking of Bitou bush.

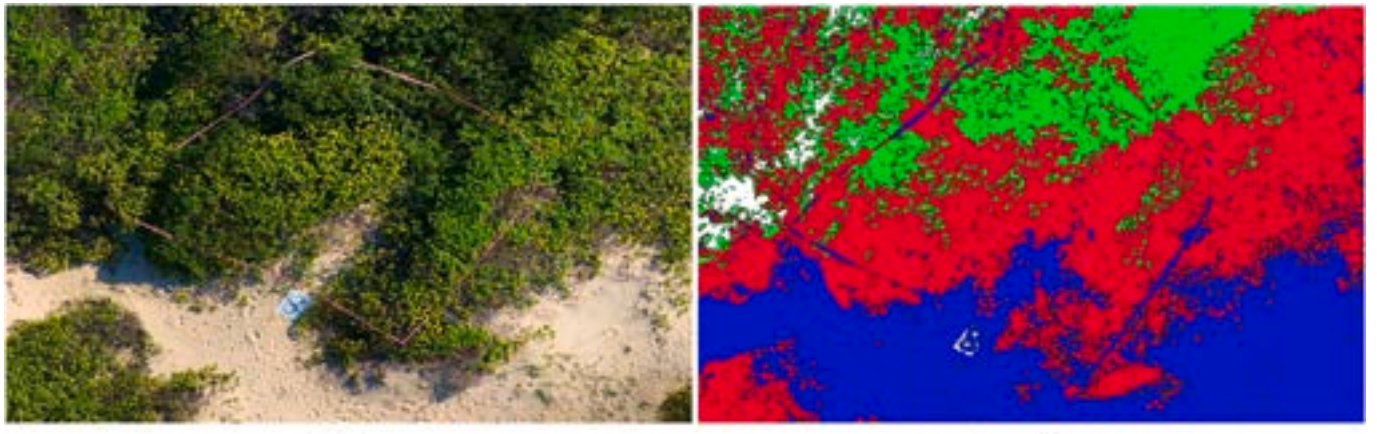

Fig. 11. (a) Region of interest of multispectral imagery; (b) Semi-automatic labelled region of interest using thresholding techniques: Bitou bush in red colour, other vegetations in green colour and non-vegetations in blue colour. (For interpretation of the references to colour in this figure legend, the reader is referred to the Web version of this article.)

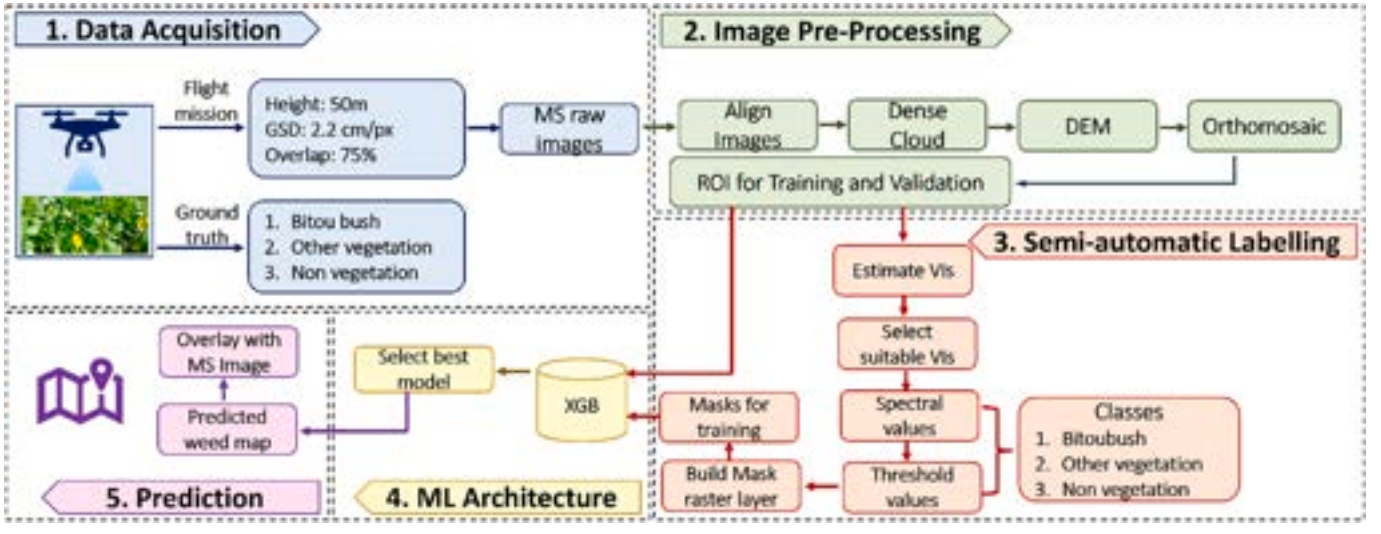

Fig. 12. Processing pipeline for bitou bush detection using semi-automatic labelling.

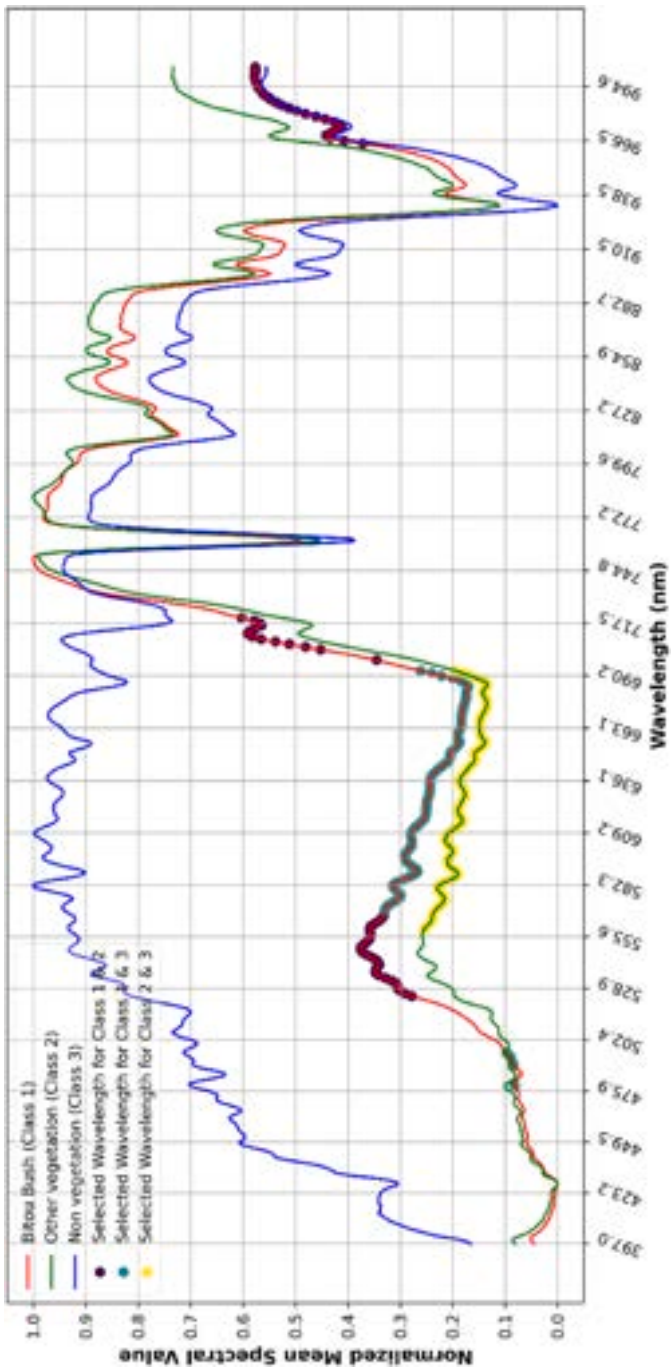

Fig. 13. Spectral signature curve for hyperspectral image for different classes used in this study.

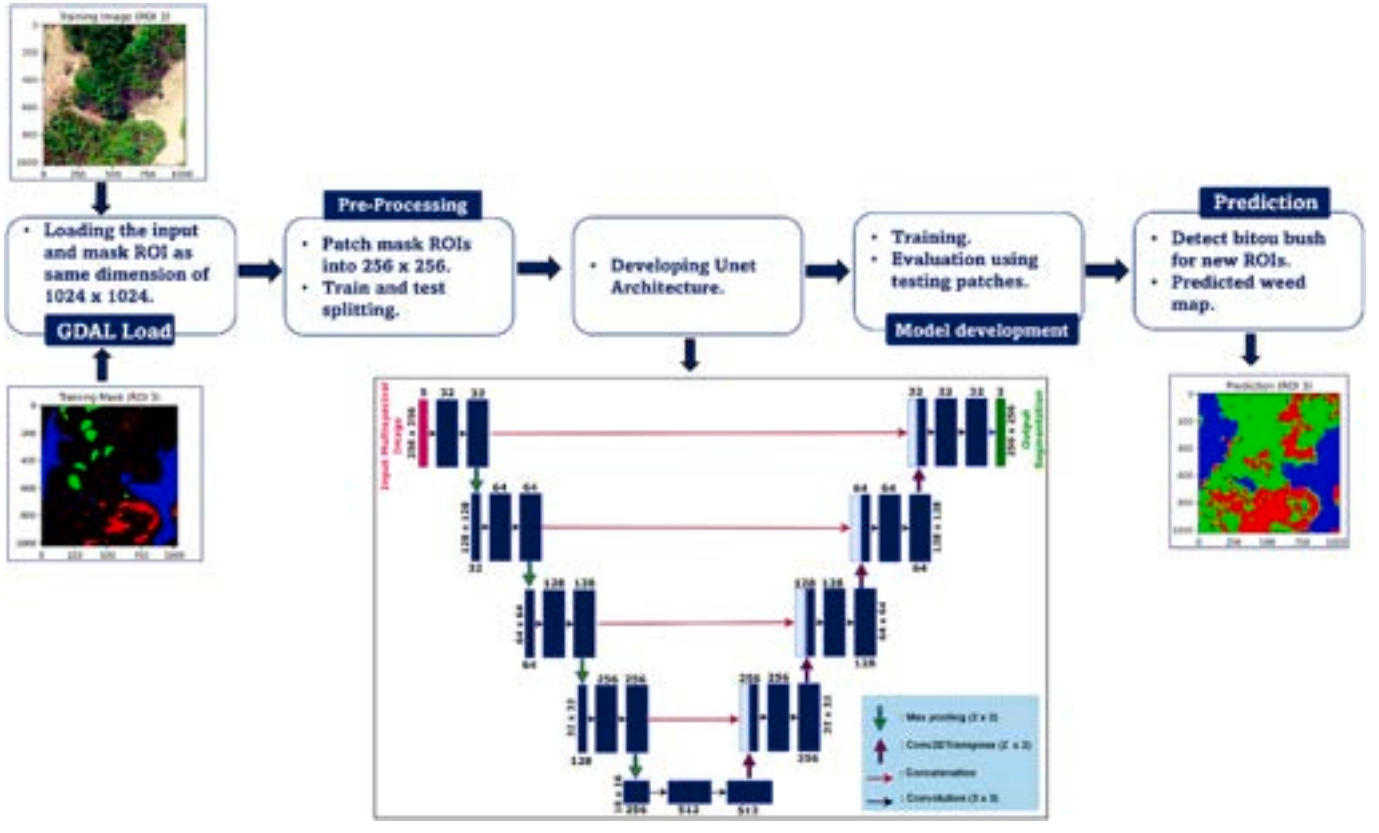

Fig. 14. U-Net processing pipeline for bitou bush mapping.

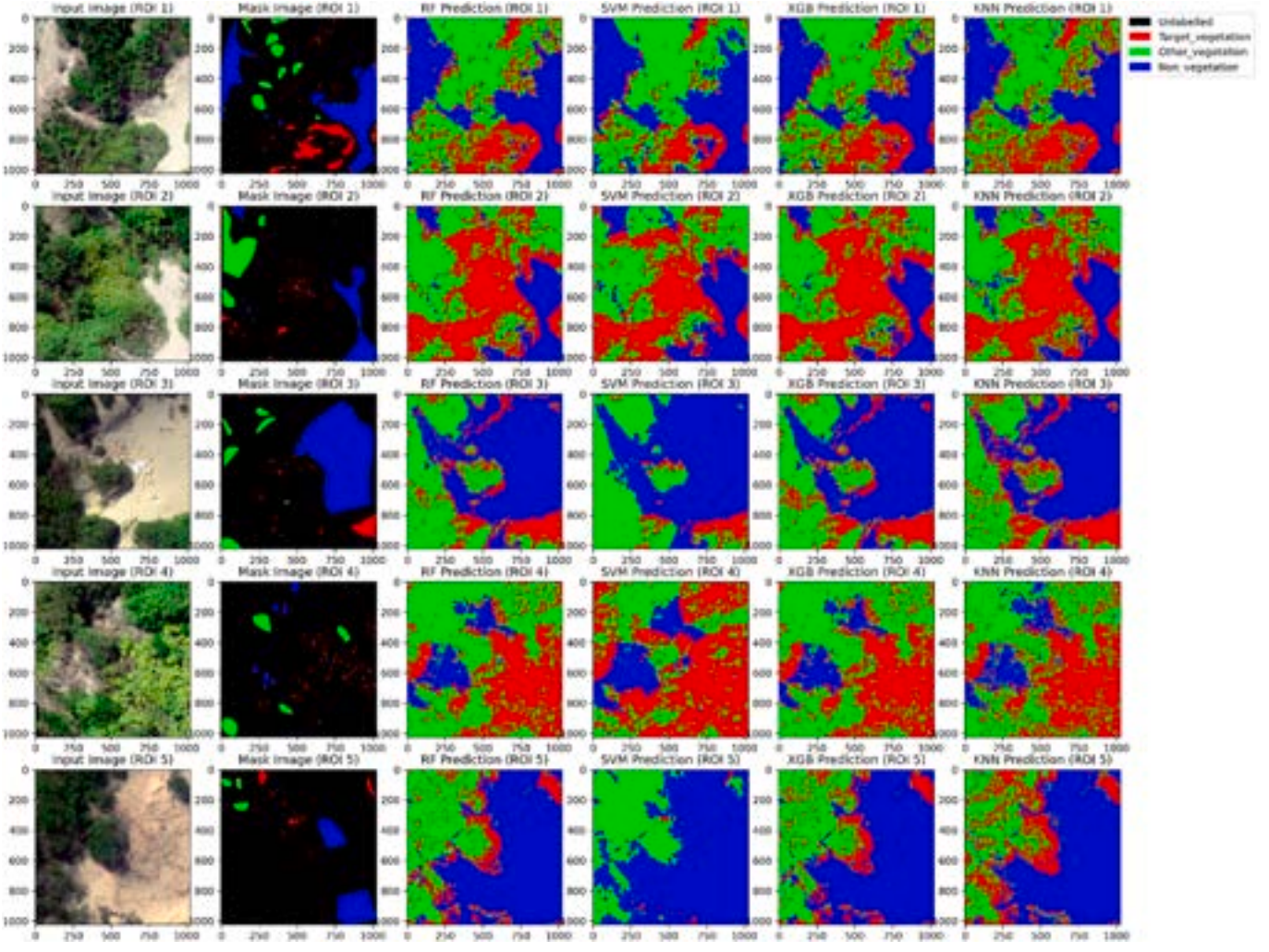

Fig. 15. Prediction results using different classical ML models for training and testing.

Table 7
Classification report for different classical machine learning models including Random forests (RF), Support vector machine (SVM), Extreme gradient boosting (XGB), and K-nearest neighbors (KNN) for training and testing at ground sampling distance (GSD) of 2.2cm/pixel.

Classes	Matrix	RF	SVM	XGB	KNN
Target vegetation	Precision (%)	100	82	98	100
	Recall (%)	94	77	94	100
	F_1-score (%)	97	80	96	100
Other vegetation	Precision (%)	93	77	93	100
	Recall (%)	100	70	98	100
	F_1-score (%)	96	74	95	100
Non-vegetation	Precision (%)	100	86	99	100
	Recall (%)	99	98	98	100
	F_1-score (%)	99	92	99	100
Overall accuracy of model (%)		98	82	97	100

enhancement, efficient training, and optimized resource allocation. Striking a harmonious balance between informative spectral features and computational efficiency, this approach culminated in the creation of robust, accurate, and interpretable ML models.

2.6.1. Classical machine learning models training

A methodology was implemented in the development of classical ML, including XGB, RF, SVM, and KNN, specifically designed for pixelwise classification. General Python libraries, such as NumPy, Matplotlib, Joblib, scikit-image, and seaborn, were imported to facilitate the initial stages of the research. Additionally, the GDAL module from the osgeo package was employed to handle geospatial data within the dataset. The data preprocessing phase involved tasks such as filtering unlabeled data, extracting features from source images, and creating labelled data variables ('X' features and 'y' labels) converted to an array format. Subsequent steps encompassed train-test split and data normalization using scikit-learn's StandardScaler for Euclidean distance. The different classical ML models (XGB, RF, SVM, KNN) were fitted to the training data. Model evaluation utilized scikit-learn functionalities for confusion matrix generation, classification reports, and an overall assessment of model performance on test data. Notably, the best model for each algorithm (XGB, RF, SVM, KNN) was saved, contributing to the comprehensive evaluation of the ML model's efficacy. In the pursuit of achieving optimal performance in classical ML tasks, model selection and hyperparameter tuning play pivotal roles. Among the various models explored, the best-performing model was identified using specific hyperparameters. The RF Classifier exhibited good performance with a configuration defined by "n_estimators" = 150, and "max_depth" = 16. SVM utilized a radial basis function (RBF) kernel, adding flexibility to capture complex relationships within the data. The XGB Classifier, an implementation of gradient-boosted decision trees, demonstrated its efficacy with an objective set to "multi:softmax", and "n_estimators = 100". Additionally, the KNN Classifier, a non-parametric and instance-based learning algorithm, was fine-tuned with "n_neighbors" = 5.

2.6.2. U-Net deep learning model training

The initial phase involves importing essential Python libraries, including NumPy, OS, Pandas, OpenCV, Matplotlib, Seaborn, scikit-image for image processing, TensorFlow and Keras for model training and scikit-learn for model evaluation. Geospatial data handling was facilitated by importing GDAL. Following this, images (16 ROIs) and respective masks are tiled based on user-specified dimensions mentioned in Table 4, with corresponding paths and directories established for data retrieval. The process continued with the conversion of mask data to categorical representation through one-hot encoding, preparing it for segmentation analysis. A critical step involved splitting the dataset into training and testing sets using scikit-learn's train_test_split function. The U-Net architecture (Fig. 14), featuring convolutional and deconvolutional layers along with skip connections, was defined to facilitate semantic segmentation. The model is compiled using the Adam optimizer and categorical cross-entropy loss, and subsequently trained on the training data, with model checkpoints saved based on validation loss. To evaluate the model's performance, confusion matrices and classification reports were generated by predicting on the test data. Furthermore, Intersection over Union (IoU) calculations are performed for each class in the segmentation, providing a quantitative measure of segmentation accuracy. Many model architectures were employed, each with varying characteristics such as the number of convolution layers, kernel sizes and dropout rates. Also, different number of learning

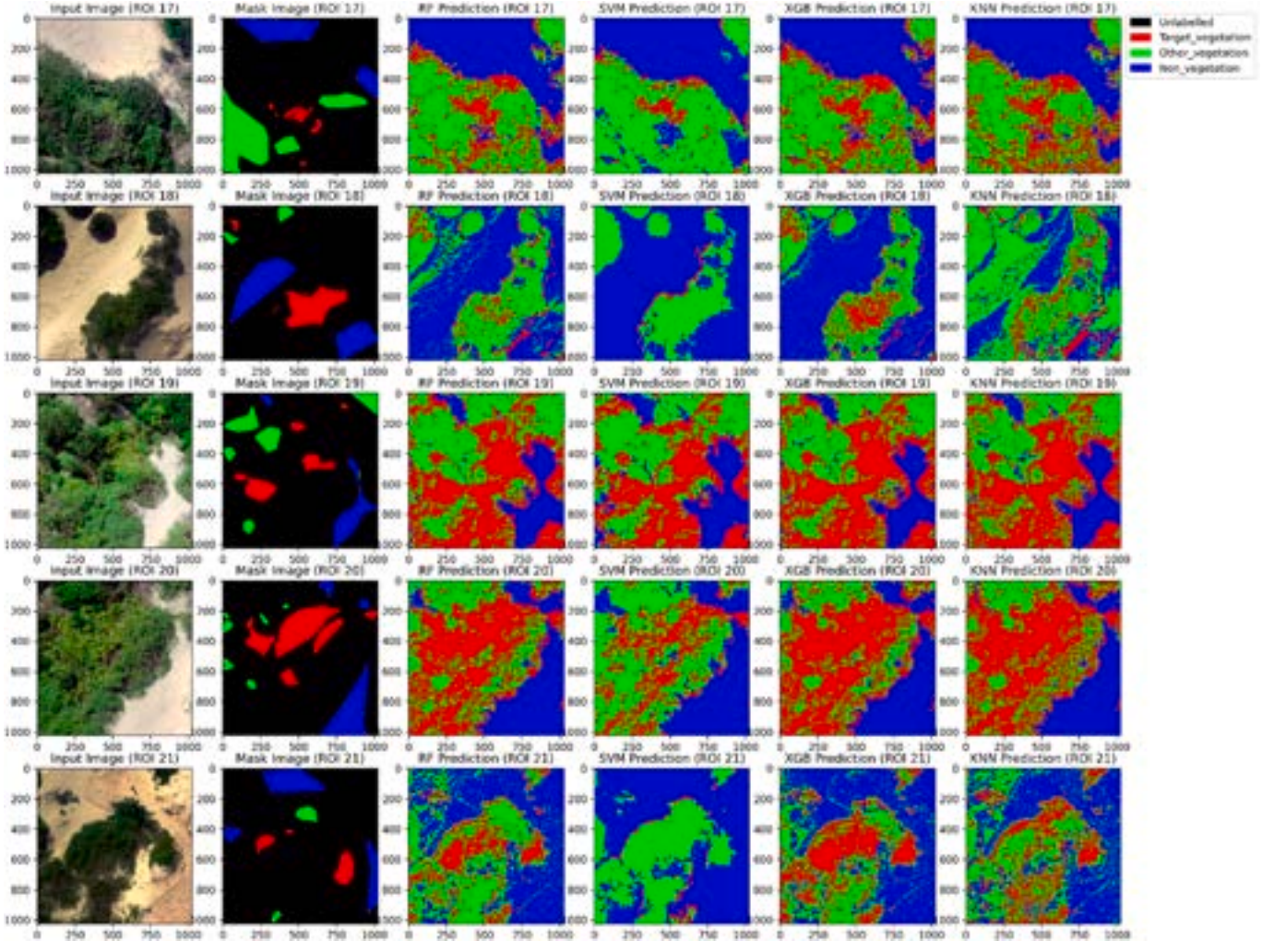

Fig. 16. Prediction results of ROIs (Id 17 to 21) using different classical ML models for validation.

Table 8
Classification report for different classical machine learning models including Random forests (RF), Support vector machine (SVM), Extreme gradient boosting (XGB), and K-nearest neighbors (KNN) for validation at ground sampling distance (GSD) of 2.2cm/pixel.

Classes	Matrix	RF	SVM	XGB	KNN
Target vegetation	Precision (%)	79	90	75	68
	Recall (%)	63	40	72	64
	F_1-score (%)	70	55	74	66
Other vegetation	Precision (%)	67	60	73	56
	Recall (%)	80	85	74	69
	F_1-score (%)	73	71	73	62
Non-vegetation	Precision (%)	92	86	92	90
	Recall (%)	91	99	95	75
	F_1-score (%)	91	92	93	82
Overall accuracy of model (%)		78	74	80	69

rates, batch sizes, and the number of epochs were used for model training and tuning. The optimal configuration for the bitou bush segmentation model involves using 5 bands, a patch size of 256, and a train-test split of 25%. Additionally, the recommended convolution layers range from 32 to 512, with a dropout rate of 0.2, a learning rate of 0.001, and a batch size of 25, with training epochs set at 200 for optimal performance.

2.7. Evaluation metrics

Finally, the predicted map and labelled map were aligned with the actual MS and HS raster and the accuracy of the expected outcome was confirmed by weed specialists. The classification report was developed to compare and evaluate the detection performance of the different classical ML models and DL U-Net model. Evaluation metrics, including true positives (TP), false positives (FP), true negatives (TN), and false negatives (FN) were used to calculate the overall accuracy (Equation (1)), precision (Equation (2)), recall (Equation (3)), F_1-score (Equation (4), and Intersection over Union (IoU) (Equation (5).

$$\text{Overall Accuracy} = \frac{TP + TN}{TP + TN + FP + FN} \tag{1}$$

$$\text{Precision} = \frac{TP}{TP + FP} \tag{2}$$

$$\text{Recall} = \frac{TP}{TP + FN} \tag{3}$$

$$F_1\text{-score} = \frac{2TP}{FP + 2TP + FN} \tag{4}$$

$$\text{Intersection over Union (IoU)} = \frac{Area\ of\ intersection}{Area\ of\ Union} \tag{5}$$

3. Results

3.1. Performance of classical machine learning models using multispectral imagery

3.1.1. Performance of training and testing dataset

Fig. 15 shows the prediction results of different ROIs using different classical ML models during training and testing. The models are assessed based on precision, recall, and F_1-score for three target classes including target vegetation, other vegetation, and non-

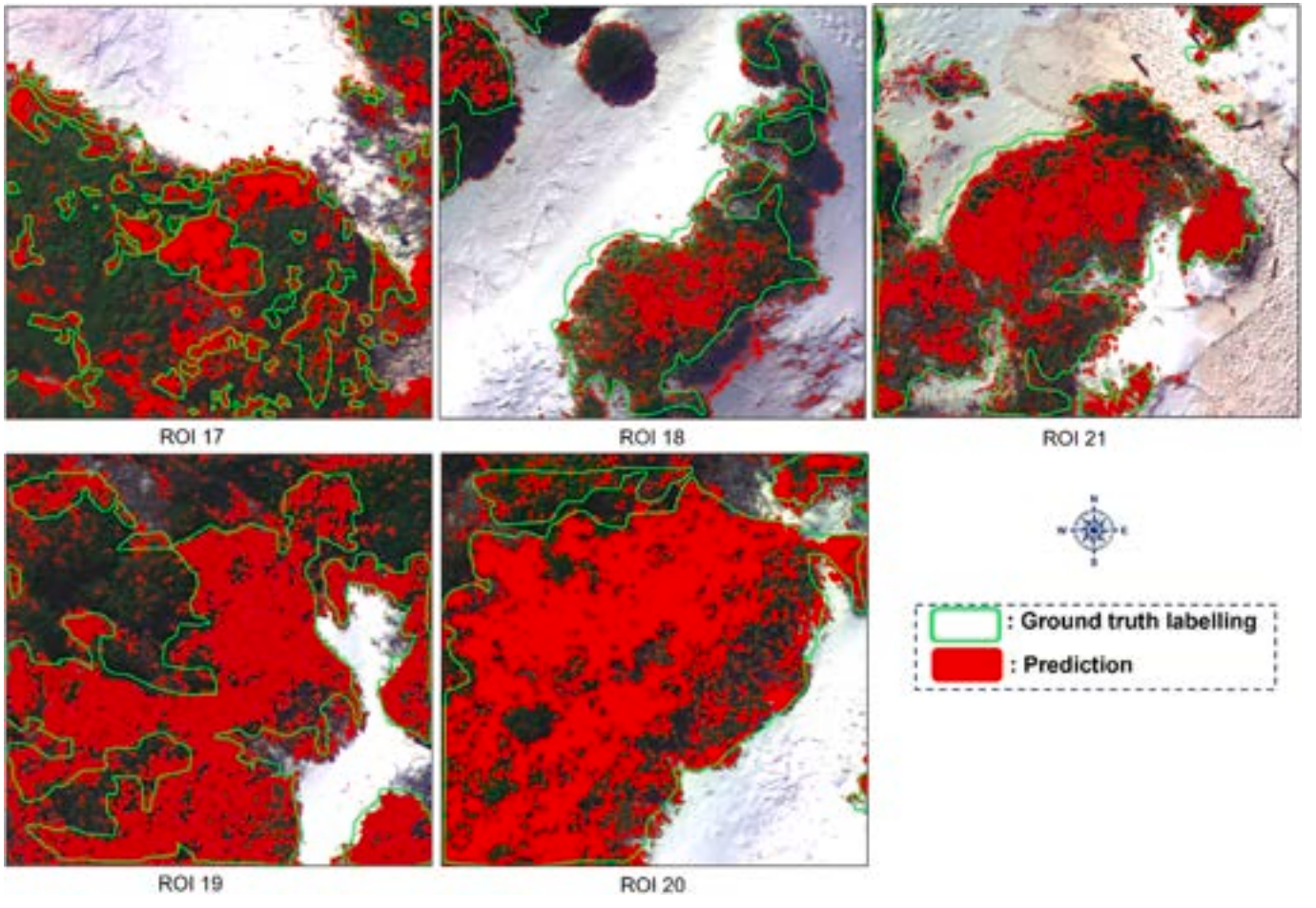

Fig. 17. Comparison of the XGB model prediction against ground truth labelling (verified bitou bush) for 5 Regions of Interest (ID 17 to 21).

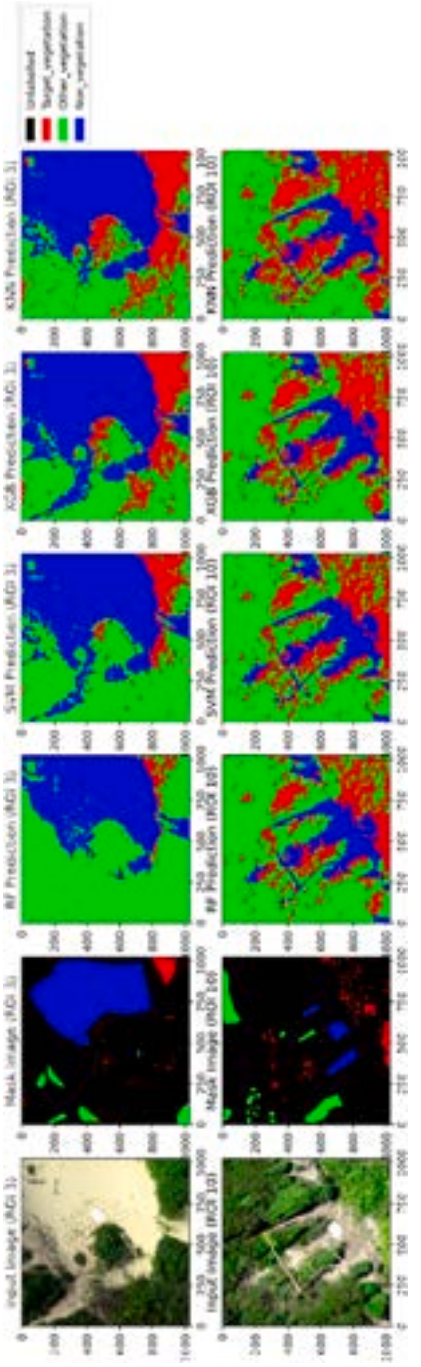

Fig. 18. Prediction results using different classical ML models for training and testing.

Table 9
Classification report for different classical machine learning models including Random forests (RF), Support vector machine (SVM), Extreme gradient boosting (XGB), and K-nearest neighbors (KNN) for training and testing at ground sampling distance (GSD) of 3.5cm/pixel.

Classes	Matrix	RF	SVM	XGB	KNN
Target Vegetation	Precision (%)	98	97	100	100
	Recall (%)	70	88	98	100
	F_1-score (%)	82	93	99	100
Other Vegetation	Precision (%)	75	89	98	100
	Recall (%)	99	97	100	100
	F_1-score (%)	85	93	99	100
Non-Vegetation	Precision (%)	100	99	100	100
	Recall (%)	97	99	100	100
	F_1-score (%)	98	99	100	100
Overall accuracy of model (%)		88	95	99	100

vegetation (Table 7). KNN exhibits the best performance overall, achieving 100% precision, recall, and F_1-score for target vegetation and non-vegetation classes. RF and XGB also demonstrate competitive performance, with RF achieving 98% overall accuracy and XGB achieving 97% overall accuracy. SVM is less superior, with an overall accuracy of 82%.

3.1.2. Performance of validation dataset

Fig. 16 shows the prediction results of different ROIs using different classical ML models during validation. Among the models, SVM achieved the highest precision for target vegetation, scoring 90%. However, XGB showed the best recall and F_1-score with 72% and 74% respectively for the same class. For other vegetation, XGB demonstrated the highest precision and F_1-score at 73%, while SVM had the highest recall at 85%. In the non-vegetation class, XGB obtained the highest precision and F_1-score at 92% and 92%, respectively. Overall accuracy was highest for XGB at 80%, followed closely by RF and SVM at 78% and 74%, respectively (Table 8). Fig. 17 compares prediction results from the selected best model (XGB) and ground truth labelled regions for each validation ROIs.

3.2. Performance of classical machine learning models using hyperspectral imagery

3.2.1. Performance of training and testing datatset

Fig. 18 shows the prediction results across all ROIs using different classical ML models during training and testing. For all target classes (target vegetation, other vegetation, and non-vegetation), the models RF, SVM, XGB, and KNN achieve overall accuracies, of 88%, 95%, 99%, and 100% respectively (Table 9).

3.2.2. Performance of validation dataset

Fig. 19 shows the prediction results across all ROIs using different classical ML models during training and testing. Both SVM and XGB achieved the highest overall accuracy at 86%, while RF and KNN obtained overall accuracies of 77% and 80% respectively (Table 10). Fig. 20 compares prediction results from selected best models (XGB and SVM) and ground truth labelled regions for each validation ROIs.

3.3. Comparison of predictions using multispectral and hyperspectral imagery

Fig. 21 presents a comparative analysis of prediction results derived from the use of two selected models, namely XGB for MS data and RF for HS data. The selection of these models was based on rigorous evaluation using validation accuracy as the primary criterion.

3.4. Performance of U-Net model using multispectral imagery

3.4.1. Performance of training and testing dataset

Fig. 22 shows the prediction results of different ROIs using U-Net during training and testing. For the class target vegetation, U-Net achieved a precision of 88%, recall of 89%, and F_1-score of 88%, indicating its ability to accurately identify this class. Similarly, for other vegetation, the model achieved a precision of 83%, recall of 87%, and F_1-score of 85%, demonstrating its capability to distinguish this class effectively. Moreover, for non-vegetation, U-Net achieved high precision (99%), recall (97%), and F_1-score (98%), indicating its excellent performance in recognizing non-vegetation areas. Overall, the model achieved an accuracy of 98% during training and testing (Table 11).

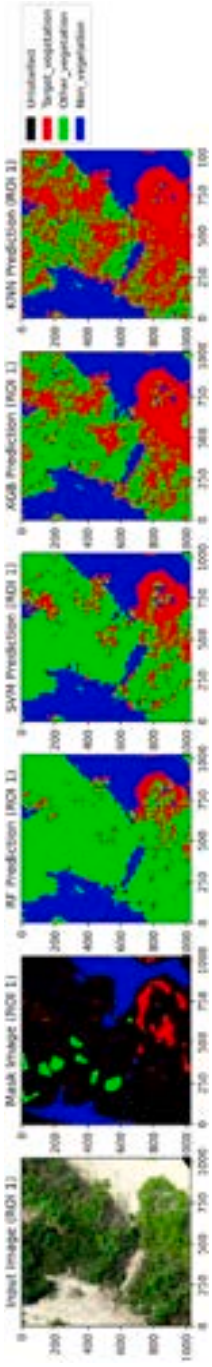

Fig. 19. Prediction results using different classical ML models for validation.

Table 10
Classification report for different classical machine learning models including Random forests (RF), Support vector machine (SVM), Extreme gradient boosting (XGB), and K-nearest neighbors (KNN) for validation at ground sampling distance (GSD) of 3.5cm/pixel.

Classes	Matrix	RF	SVM	XGB	KNN
Target Vegetation	Precision (%)	96	97	84	69
	Recall (%)	44	71	86	89
	F_1-score (%)	61	82	85	78
Other Vegetation	Precision (%)	63	77	86	85
	Recall (%)	94	91	79	56
	F_1-score (%)	76	84	83	67
Non-Vegetation	Precision (%)	88	87	89	89
	Recall (%)	92	95	94	94
	F_1-score (%)	90	91	91	91
Overall accuracy of model (%)		77	86	86	80

3.4.2. Performance of validation dataset

Fig. 23 shows the prediction results of different ROIs using the U-net model during validation. U-Net demonstrated excellent performance for all classes. It achieved 90% precision, recall, and F1-score for target vegetation. Also, it achieved 88% precision and 86% recall, with an F_1-score of 87% for other vegetation; and 95% precision, 97% recall, and a 96% F_1-score for non-vegetation. The model's overall accuracy was measured at 92%, indicating its efficacy in accurately detecting bitou bush in the study site (Table 12). Fig. 24 compares prediction results from U-Net and ground truth labelled regions for each validation ROIs.

3.5. Comparison of predictions from XGBoost and U-Net using multispectral imagery

Fig. 25 depicts the prediction results and a comparison between two models, XGB and U-Net. Both models demonstrate good performance in their respective predictions. XGB operates at a pixelwise level, independently predicting labels for individual pixels, while U-Net uses an semantic regions wise approach, segmenting the entire image into distinct semantic regions-based on learned features and assigning labels accordingly. In the XGB results, some mixed classifications are observed due to difficulties in handling mixed pixels effectively. Conversely, U-Net excels in handling mixed pixels, providing more coherent and accurate segmentation results.

3.6. Comparison of predictions from manual and semi-automatic labelling techniques

Fig. 26 illustrates the prediction results using various labelling techniques in the research study. The first subfigure (a) displays the MS ROI, serving as the ground truth image. Subfigure (b) presents the prediction results obtained from automatic labelling of classes within the ROI, while subfigure (c) shows the predictions from manual labelling techniques for the same targets. This result presents the initial findings of an ongoing study focused on exploring automatic labelling techniques to reduce manual labelling time. This technique was performed only in one ROI as the main objective was to assess the feasibility of automatic labelling in identifying bitou bush. Section 3.7 shows the prediction results comparing different labelling techniques for a ROI.

3.7. Ground truth accuracy

3.7.1. Comparison of selected models

Model performances were also tested using IoU as the validation metric between object wise ground truth labelling and predictions for different selected models in different ROIs in the validation dataset. Table 13 presents a comparative analysis of three different selected models (XGB, U-Net, and SVM) across various validation ROI and image types (MS and HS) using IoU. Notably, for MS images, U-Net consistently outperforms XGB, achieving higher IoU percentages in all ROIs and U-Net achieved 73.2% of IoU. In contrast, the SVM model, evaluated on HS data in a ROI, achieves an IoU value of 62.7%. For XGB and U-Net, both applied to MS imagery with a validation dataset covering a region of 1179.1 m^2 (bitou bush, other vegetation, and non-vegetation), XGB achieved an accurate prediction area of 253.4 m^2 for bitou bush, whereas U-Net demonstrated superiority in performance, accurately identifying 342.3 m^2 of bitou bush area. It is notable that the actual bitou bush area within the validation dataset was 382.3 m^2. In the case of the SVM model applied to HS imagery within a validation dataset of 117.7 m^2, it achieved a prediction area of 29.1 m^2 for bitou bush, with the actual bitou bush area in the dataset being 35.24 m^2. In Fig. 27, the prediction map of the study site is presented, utilizing the optimal DL U-Net model for accurate and detailed spatial delineation.

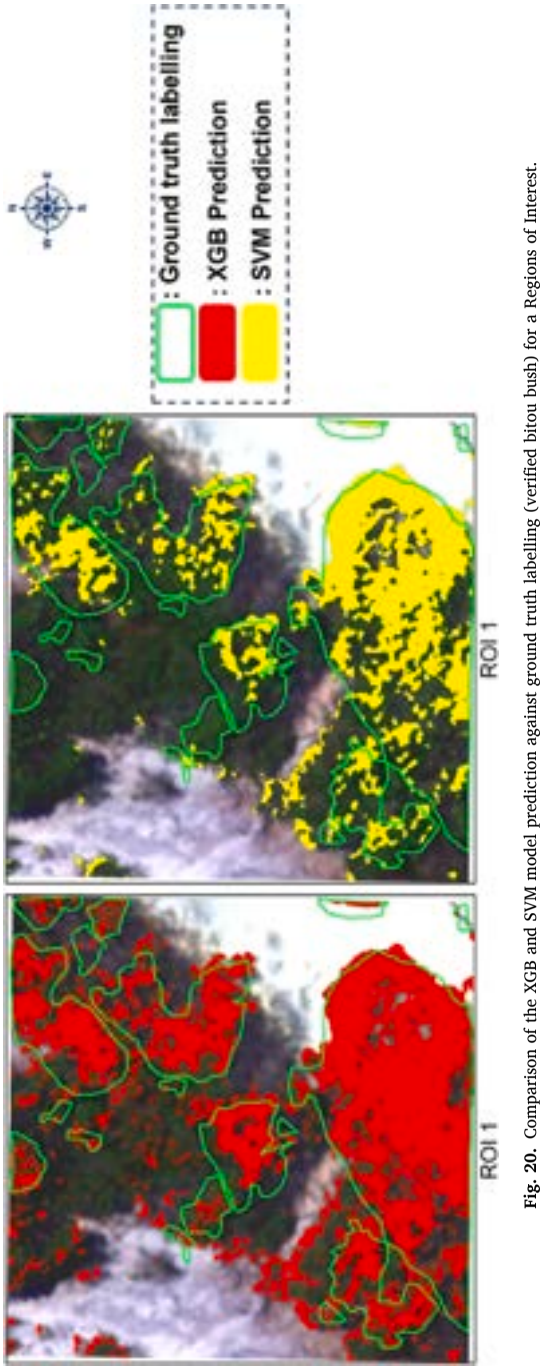

Fig. 20. Comparison of the XGB and SVM model prediction against ground truth labelling (verified bitou bush) for a Regions of Interest.

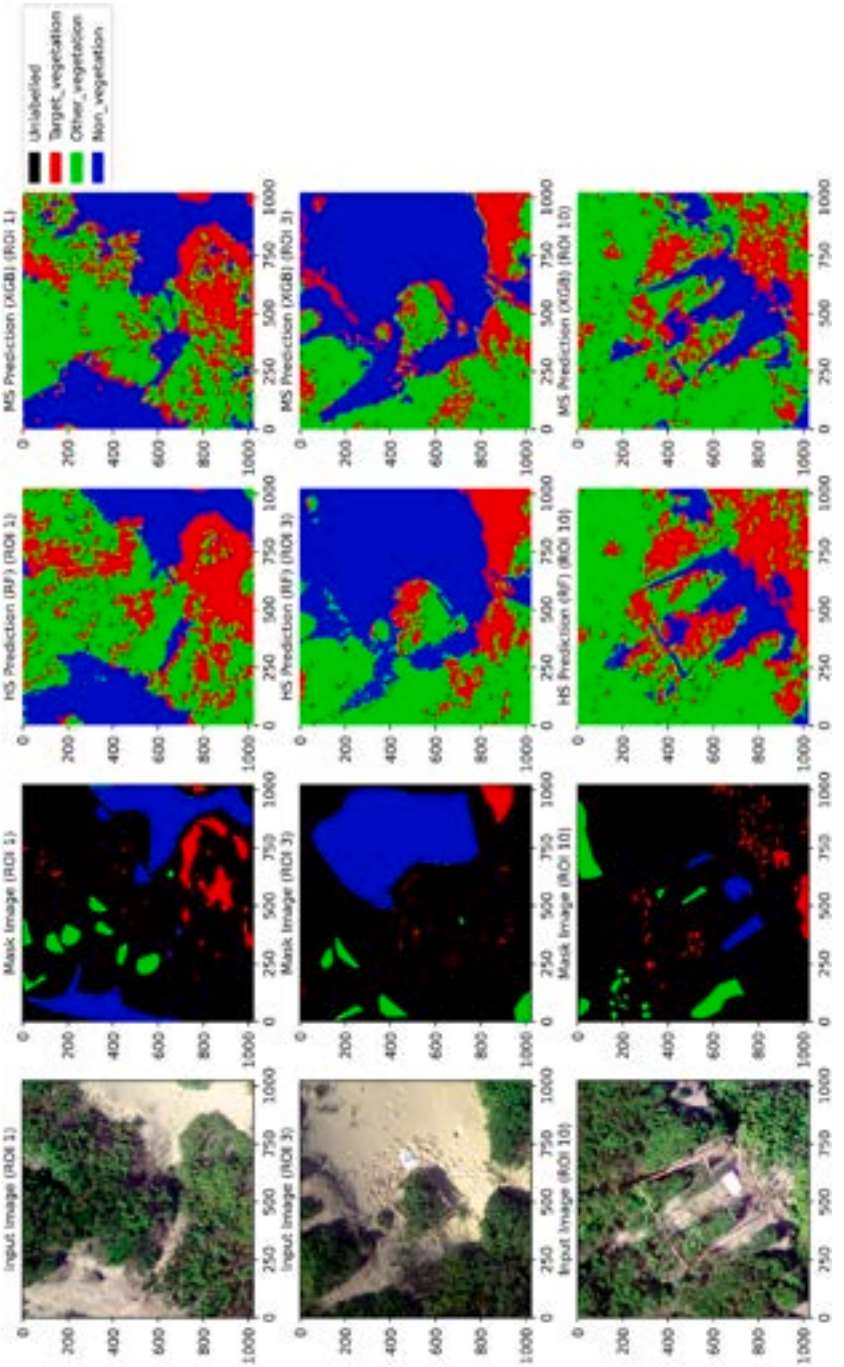

Fig. 21. Prediction results with comparison for HS images and MS images.

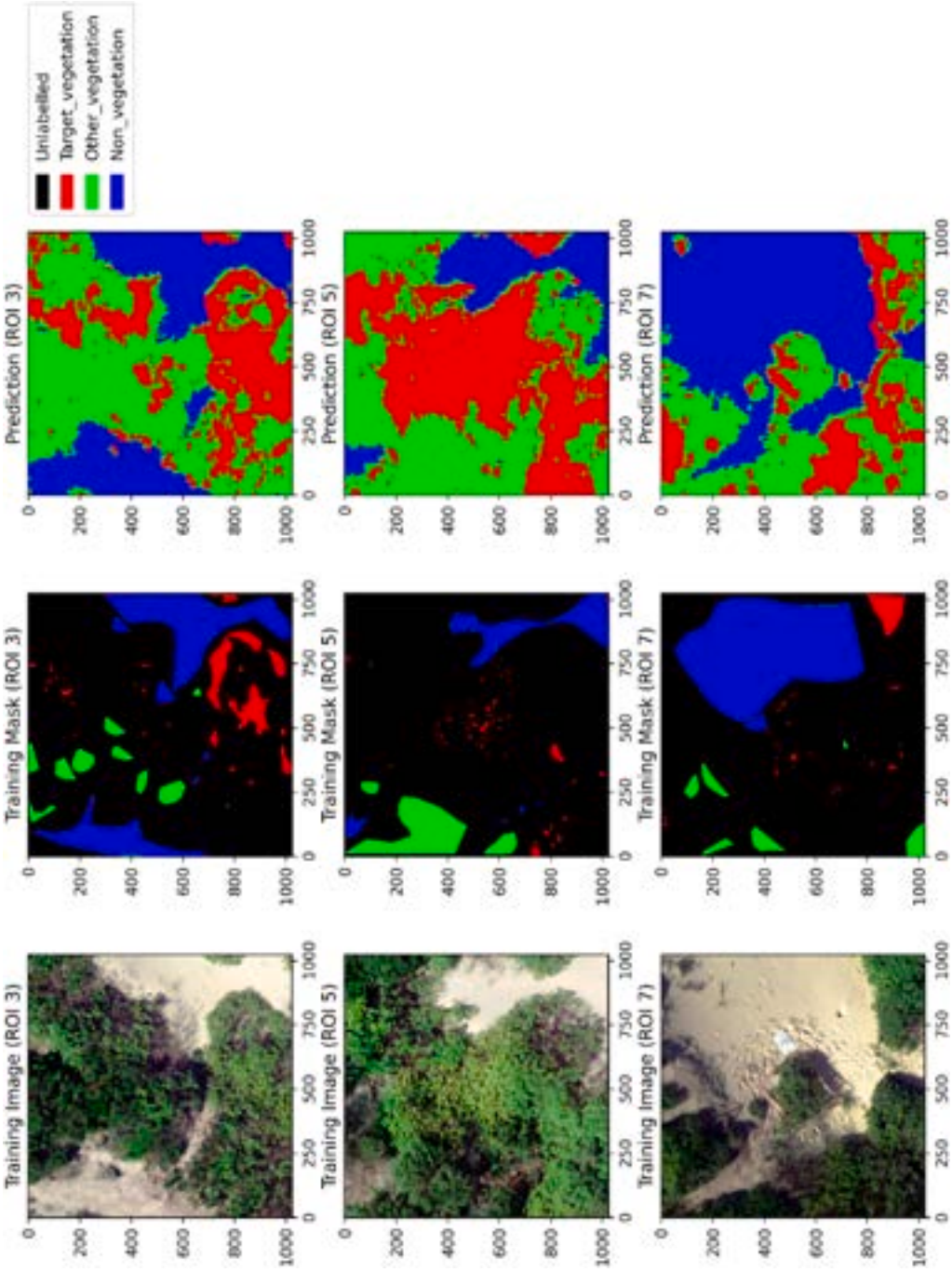

Fig. 22. Prediction results using U-Net for training and testing.

Table 11
Classification report for U-Net for training and testing at ground sampling distance (GSD) of 2.2cm/pixel.

Classes	Matrix	U-Net
Target Vegetation	Precision (%)	88
	Recall (%)	89
	F_1-score (%)	88
Other Vegetation	Precision (%)	83
	Recall (%)	87
	F_1-score (%)	85
Non-Vegetation	Precision (%)	99
	Recall (%)	97
	F_1-score (%)	98
Overall accuracy of model (%)		98

3.7.2. Comparison of different labelling techniques

Table 14 illustrates the model's performance based on the labelling methods, namely manual and semi-automatic. For the manual labelling approach, the validation dataset covered an area of 707.7 m^2, with 296.9 m^2 representing bitou bush. The XGB model trained on manually labelled data accurately predicted an area of 215.2 m^2 for bitou bush within this dataset. When employing the semi-automatic labelling method within the same validation dataset, the XGB model yielded a prediction area of 216.8 m^2 for bitou bush.

4. Discussion

The results of this study demonstrate the significant utility of ML and DL models for detecting bitou bush using MS and HS imagery in mixed environments. The superior pixel-wise prediction performance of RF, SVM, and XGB ML models using MS imagery are likely attributed to their efficiency, their generalisation capabilities on new data, their strong predictive power, and their capacity to capture complex patterns. RF excels in aggregating multiple decision trees to create robust predictions, making it well-suited for capturing the distinctive spectral signatures of bitou bush. The strength of the XGB model lies in its boosting technique, enabling it to sequentially improve on previous weak learners and achieve higher accuracy. Additionally, the ensemble nature of RF and XGB mitigates overfitting concerns that can arise in SVM and KNN, particularly when dealing with limited training samples. The feature importance and powerful regularization mechanisms offered by RF and XGB contribute to their exceptional performance, enabling more accurate detection of bitou bush, a plant which inhabits complex and heterogeneous environments. The efficacy of these models in this study are supported by the findings from different researchers who report their similar capabilities for detecting plant species in mixed landscapes (Ahmed et al., 2021; Chikuruwo et al., 2017; da Silva et al., 2023; Sandino and Gonzalez, 2018; Shiferaw et al., 2019). While KNN achieved perfect training accuracy in this study, its validation accuracy is lower compared to the other models, indicating potential challenges in generalizing to new data. Other studies have identified similar constraints with the KNN model in detection of weed species (Abeysinghe et al., 2019; Akbari et al., 2021).

The good performance of the XGB model in this study demonstrates its capacity to improving predictive accuracy by sequentially building decision trees that correct the errors of previous ones. This enables XGB to capture complex patterns and relationships in the data. These features are well suited to detecting bitou bush from heterogeneous landscapes, where differentiation between species is challenging. Other studies have also reported the superior capabilities of the XGB model and UAV MS imagery for detecting weeds from heterogeneous landscapes with high accuracy (Amarasingam et al., 2023; Sandino and Gonzalez, 2018). Contrastingly, Villoslada et al. (2020) highlighted the RF model as being more accurate than the XGB model for detection of invasive grass weeds in mixed coastal landscapes, a finding also supported by Lu and He (2017) who also achieved an overall accuracy of 85% using RF when applied to species classification in a heterogeneous grassland.

The notable performance of the SVM and XGB models for detecting bitou bush from HS imagery in this study is supported by previous research by Papp et al. (2021), who also achieved very high accuracies using SVM to monitor invasive plant species using HS imagery. However, the superiority of the XGB model performance in HS over MS imagery overall in this study was likely influenced by the inherent complexity and richness of the spectral information provided by HS images, despite constraints in HS data availability and a limited representation of the underlying scene. The greater number of spectral bands in HS images data allow the classifiers to discern finer details and subtle variations, which may have resulted in improved accuracy compared to MS images, where a more

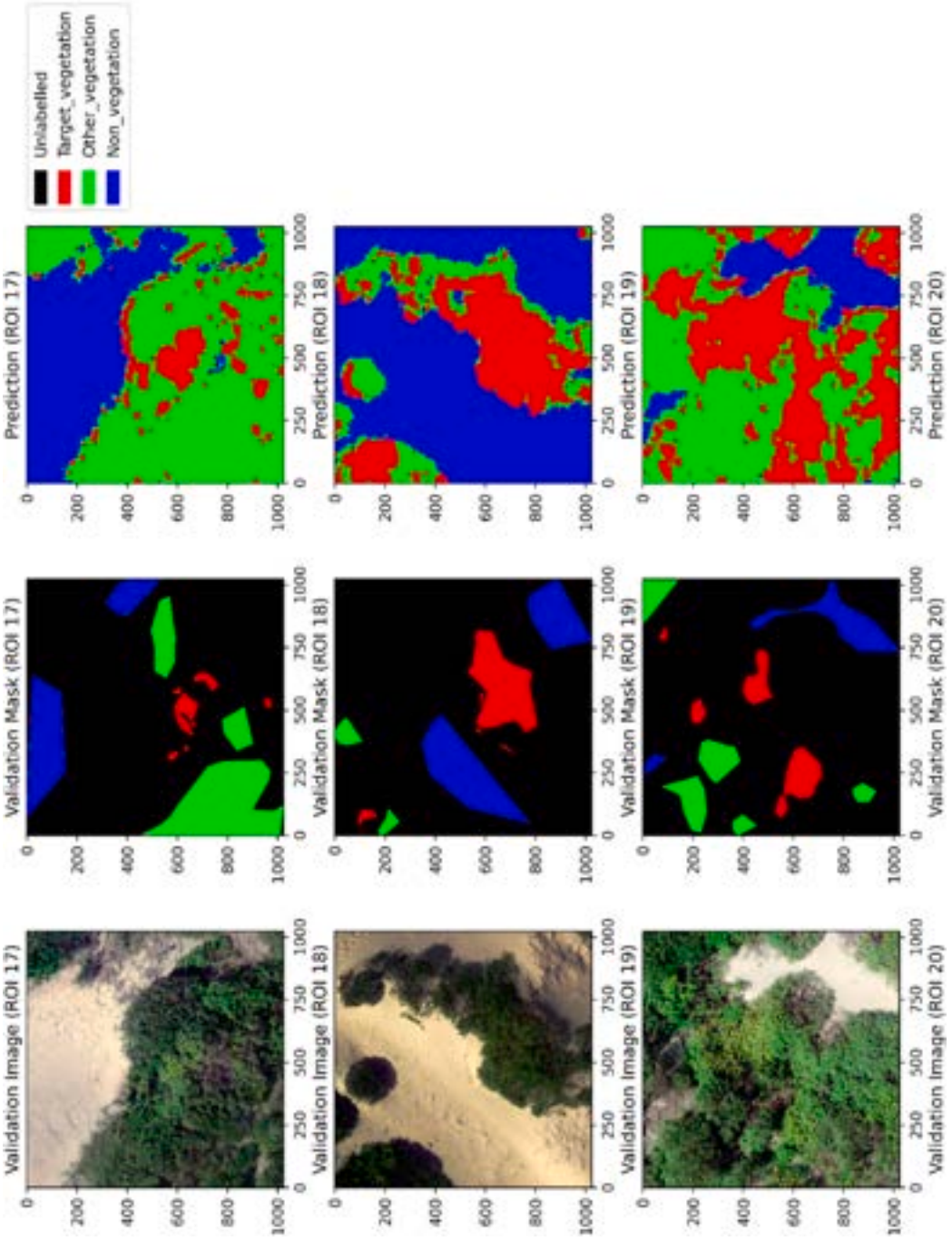

Fig. 23. Prediction results of ROIs (ID 18 to 20) using U-Net for validation.

Table 12
Classification report for U-Net for validation at ground sampling distance (GSD) of 2.2cm/pixel.

Classes	Matrix	U-Net
Target Vegetation	Precision (%)	90
	Recall (%)	90
	F_1-score (%)	90
Other Vegetation	Precision (%)	88
	Recall (%)	86
	F_1-score (%)	87
Non-Vegetation	Precision (%)	95
	Recall (%)	97
	F_1-score (%)	96
Overall accuracy of model (%)		92

comprehensive dataset and diverse representation of the landscape was acquired. These findings shed light on the potential advantages of HS images for specific classification tasks and emphasize the importance of carefully considering dataset properties when selecting appropriate classifiers for RS applications.

However, HS techniques come with disadvantages such as higher costs, increased data volume, and potential compromises in spatial resolution. In contrast, MS sensors are more cost-effective, easier to manage, and often provide better spatial resolution, making them suitable for applications where a balance between spectral and spatial information is crucial. The choice between the two sensor types depends on the specific needs of the application, considering factors like budget constraints, computational resources, and desired resolution. If high spatial resolution and detailed mapping are paramount, MS sensors may be preferred. Conversely, if the focus is on detailed spectral information for material identification, HS sensors become more advantageous. Based on results, MS imagery produced sufficient results for bitou bush mapping suggests that the use of MS sensors has proven effective in this specific application.

The greater accuracy of the U-Net DL model over all other classical ML models demonstrates that it generalizes well to new data. This is a promising result for land managers who may wish to use it to detect bitou bush at other sites, since it suggests that the model can effectively segment bitou bush in new images that it hasn't encountered during training. Similar results have been reported in other studies investigating coastal wetland vegetation classification using RF and U-Net models using RGB imagery (Zheng et al., 2022), achieving overall accuracies of 81.47% and 94.43% respectively. In contrast, several other studies report less accurate results from using different DL techniques to advance the field of vegetation and plant species detection. Detka et al. (2023) achieved between 83% and 91% accuracy from DL models when mapping various tree and shrub species, while Retallack et al. (2022) explored various CNN architectures, including YOLOv3 and Faster R–CNN, and achieved an overall accuracy of 75% in the detection of pearl bluebush. Furthermore, RF, XGB, SVM and KNN inherently operates on a pixel-wise level. As a result, its predictions might exhibit scattered pixel labelling, especially in cases where objects are not well-defined or distinct in the input data. By comparing U-Net's predictions with the ground truth data, weed experts evaluated the model's accuracy and confirmed the more superior performance of U-Net in prediction. The coherent and accurate segmentations produced by U-Net model match the ground truth information closely, indicating that the model is capable of identifying and delineating objects with high precision.

The MS nature of the imagery provides the necessary spectral information for vegetation analysis, and the combination with a U-Net model enhances the capability to accurately classify and map bitou bush. Therefore, MS imagery combined with a U-Net model can be a highly effective and practical possibility for bitou bush mapping, maximising the strengths of both components. The results of this study also highlight the potential value of semi-automatic labelling techniques for training XGB model and for determining ground truth accuracy (measured by IoU score). Pixelwise ground truth labelling is a less practical way to labels all the pixels in all ROIs in MS and HS imagery and was thus found to be a less efficient technique. Therefore, object wise ground truth labels were used to estimate IoU. However, XGB model was trained as pixelwise classification as a results XGB model from semi-automatic labelling technique was obtained lower IoU results. Additionally, the lower IoU score demonstrates that it struggles to accurately identify the boundaries of objects in the dataset. Therefore, U-Net is likely to perform better than classical ML models when using semi-automatic labelling techniques. Therefore, training using different DL models with many ROIs and different performance analyses will be the next steps for determining the utility of semi-automatic labelling in practice. Since refinement of these techniques can lead to improved model performance (Huang et al., 2015).

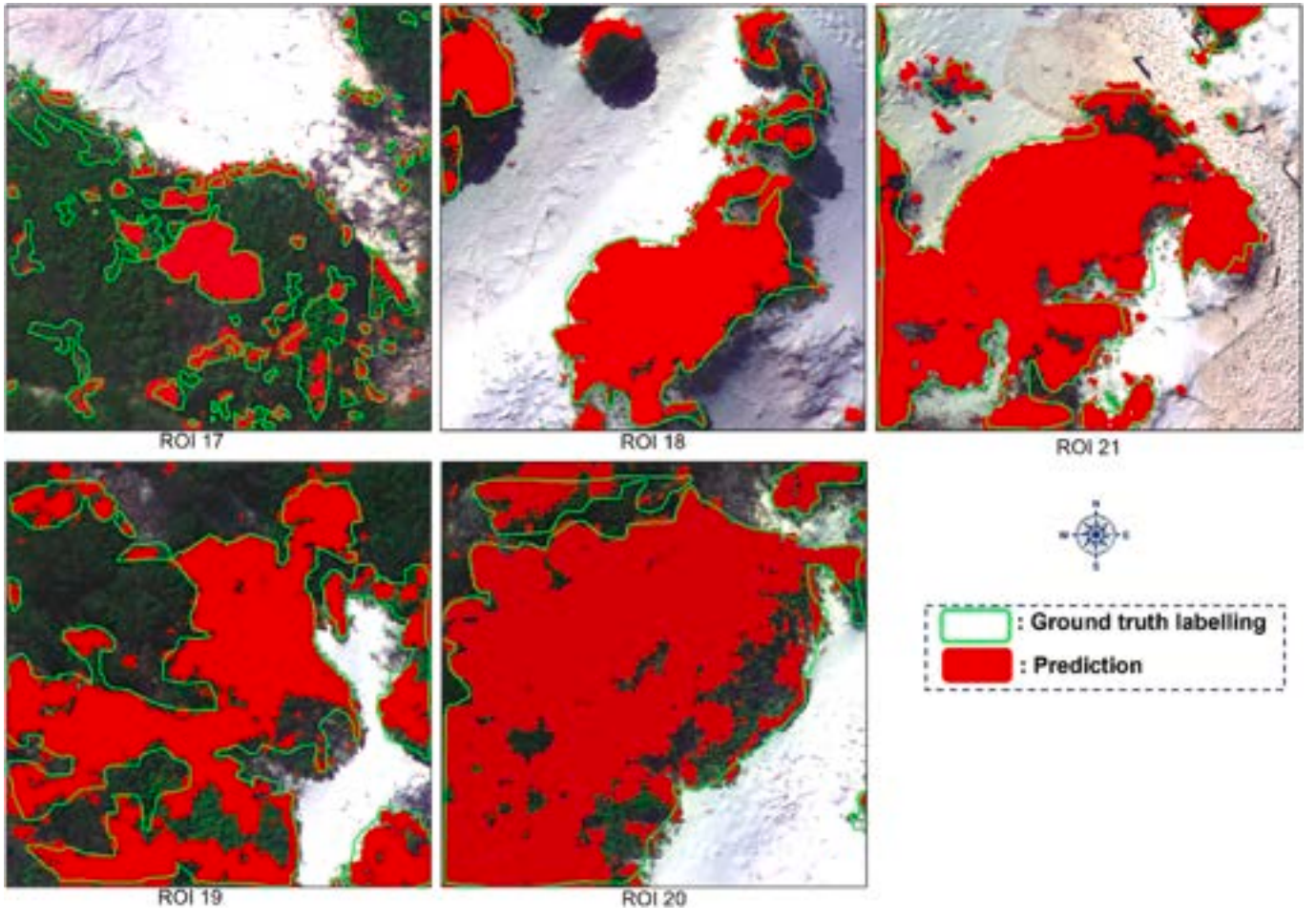

Fig. 24. Comparison of the U-Net model prediction against ground truth labelling (verified bitou bush) for 5 Regions of Interest (ID 17 to 21).

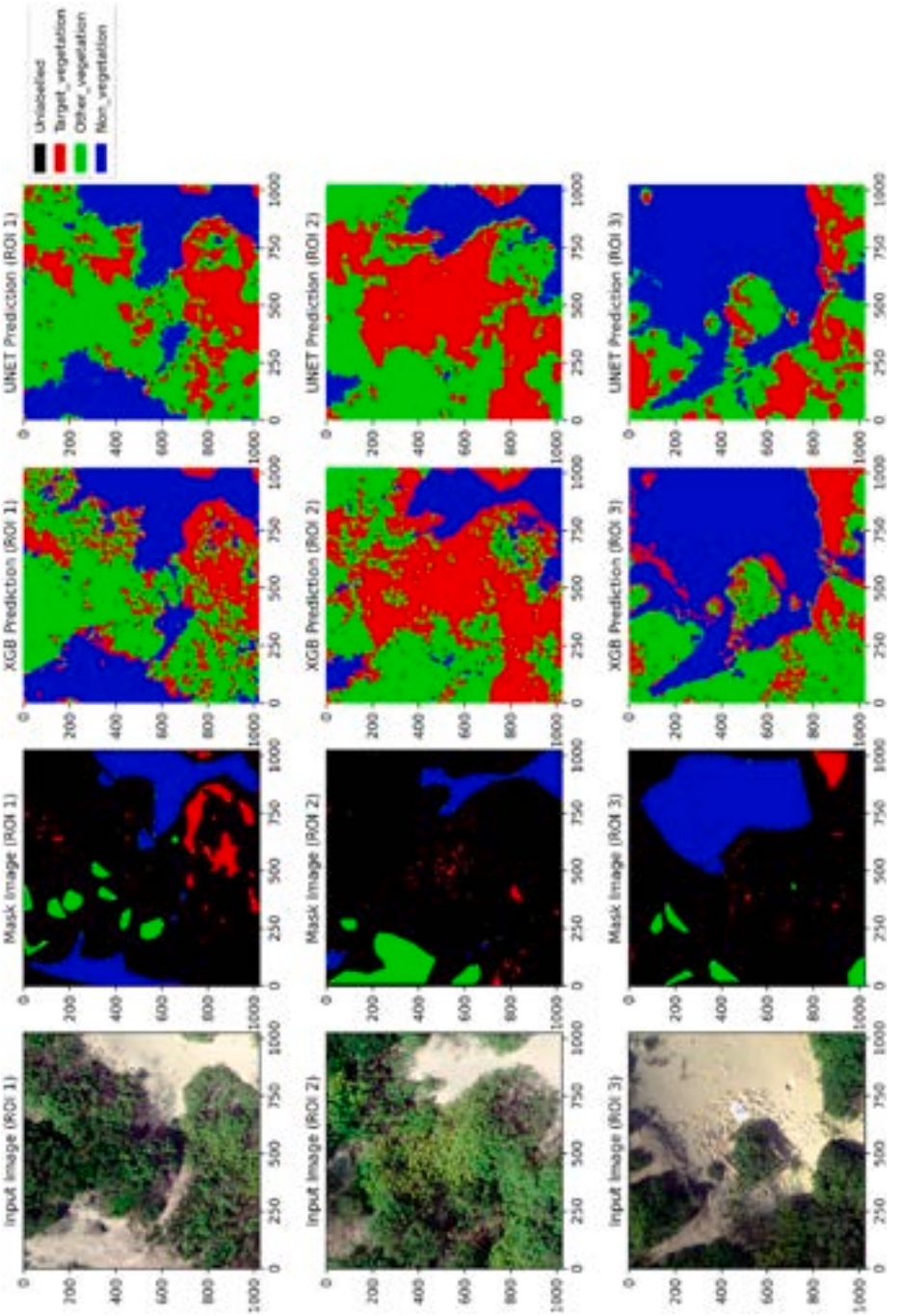

Fig. 25. Prediction results with comparison for XGB and U-Net.

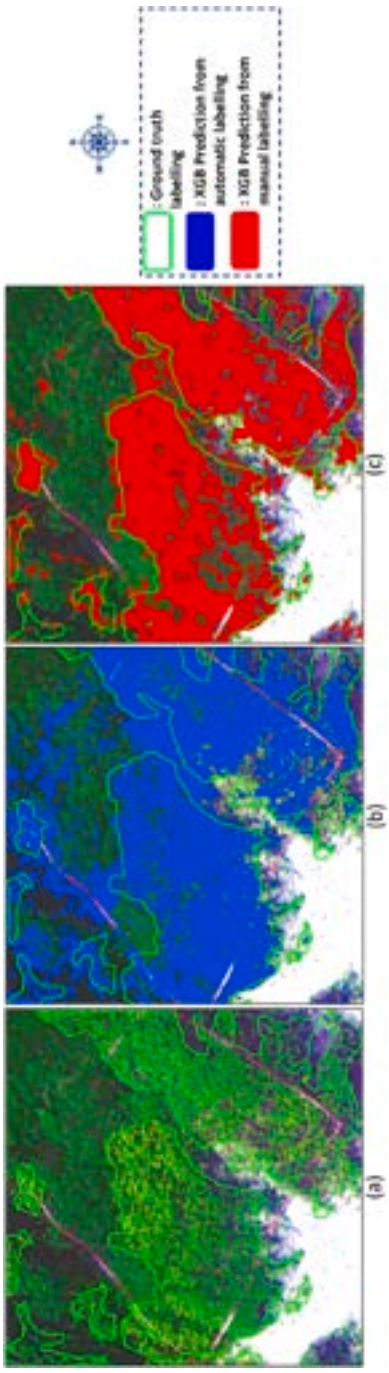

Fig. 26. Prediction results comparing different labelling techniques: (a) MS ROI; (b) Prediction from automatic labelling; (c) Prediction from manual labelling.

Table 13
Intersection of union (IoU) between ground truth and prediction for different selected models at a ground sampling distance (GSD) of 2.2cm/pixel.

Model	Image	ROI	Area (m^2)	Area of bitou bush (m^2)	Ground truth and prediction (m^2)			
					Intersection (m^2)	Union (m2)	IoU (%)	Mean IoU (%)
XGB	MS	17	235.7	28.9	18.3	64.14	28.5	46.1
		18	235.7	56.5	19.9	64.25	30.9	
		19	236	89.6	76.9	128.6	59.8	
		20	235.7	123.7	92.7	145.9	63.5	
		21	236	83.6	45.6	95.6	47.7	
U-Net	MS	17	235.7	28.9	18.2	35.9	50.8	73.2
		18	235.7	56.5	50.5	63.5	79.8	
		19	236	89.6	81.4	105.7	77.1	
		20	235.7	123.7	113.4	142.8	79.4	
		21	236	83.6	78.8	99.3	79.2	
SVM	HS	1	117.7	35.24	29.1	46.4	62.7	62.7

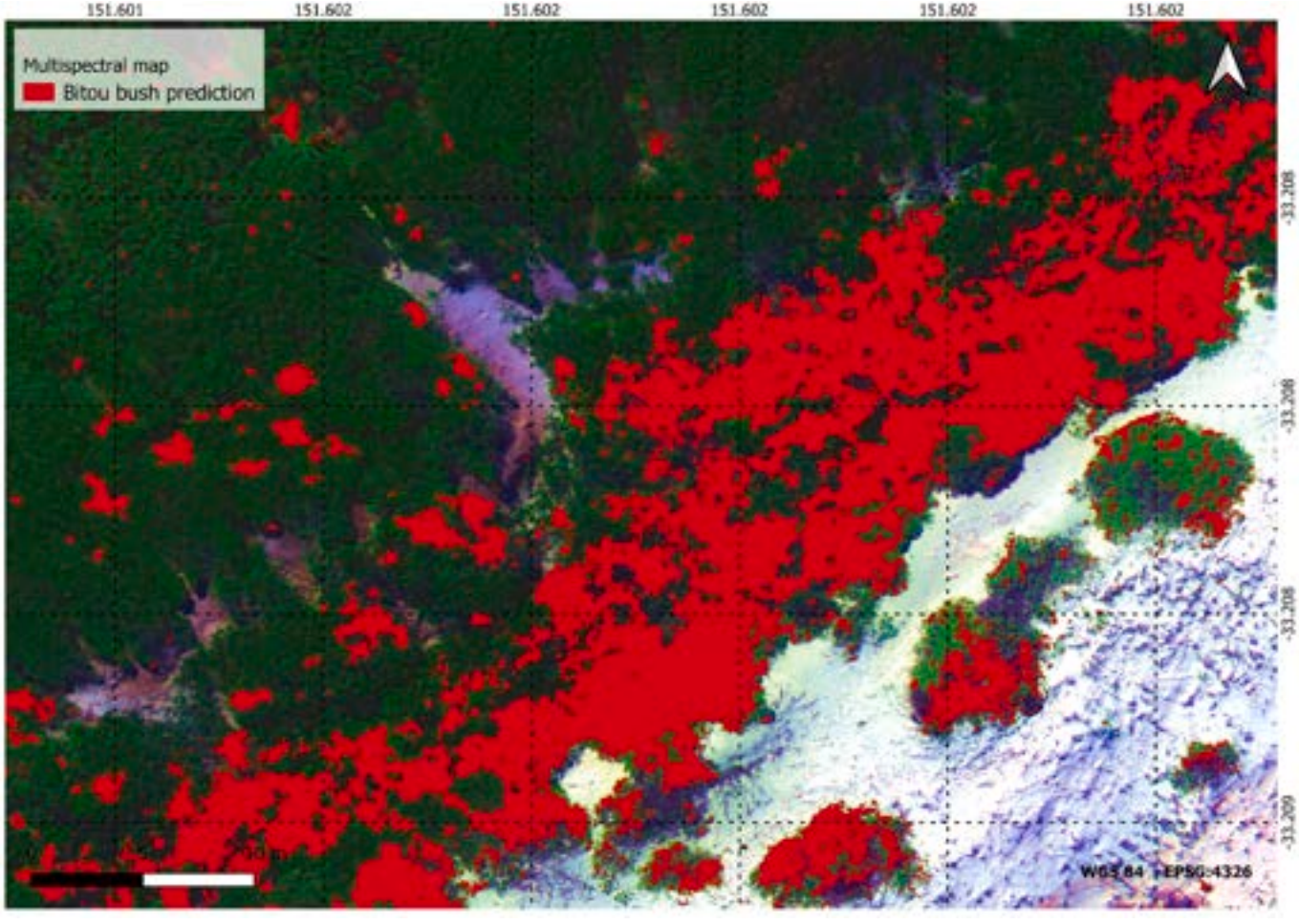

Fig. 27. Prediction map of study site using the selected best model of deep learning U-Net.

Table 14
Intersection of union (IoU) between ground truth and prediction for different labelling techniques with Extreme gradient boosting (XGB) in multispectral Regions of Interest (ROIs) at ground sampling distance (GSD) of 2.2cm/pixel.

Labelling Technique	ROI	Area (m^2)	Area of bitou bush (m^2)	Ground truth and prediction (m^2)			
				Intersection (m^2)	Union (m^2)	IoU (%)	Mean IoU (%)
Manual	19	236	89.6	76.9	128.6	59.8	57.1
	20	235.7	123.7	92.7	145.9	63.5	
	21	236	83.6	45.6	95.6	47.7	
Semi-automatic	19	236	89.6	68.4	159.8	42.8	52.7
	20	235.7	123.7	93.8	164.7	56.9	
	21	236	83.6	54.6	93.6	58.4	

5. Conclusions

This research demonstrates the significant potential of AI techniques for advancing RS applications in environmental landscapes and specifically highlights the most effective AI models for remotely-acquired MS and HS imagery and their comparative performance in detecting bitou bush in a complex landscape. Results also demonstrate the potential of automatic labelling techniques for creating efficiencies in determining ground truth accuracy. In developing a bitou bush detection model using classical ML and DL techniques on MS and HS imagery, the evaluated ML models, RF, SVM, XGB, and KNN, showed promising results in bitou bush detection using MS and HS data, while the DL U-Net model performance was found to be superior when applied to MS data classification tasks. U-Net's semantic regions-based prediction approach demonstrated superior handling of mixed pixels, providing more coherent and accurate segmentation results, while the use of automatic labelling techniques using VIs for the segmentation and mapping of weeds showed promising initial results for efficient and automated identification of bitou bush. Insights gained from this study will prove invaluable for the selection of appropriate models tailored to the unique complexities and characteristics of RS datasets.

Improving the accuracy and deployment of existing models and developing recommendations for the use of RS technology across various airborne platforms will be beneficial into the future for those wishing to implement remote weed detection in mixed landscapes. Testing model applicability to new sites, employing automatic labelling techniques, and the usefulness of various DL approaches will also require further investigation. It is important to note that this model and the results presented cannot be broadly applied at other sites with similar results. Bitou bush occurs across large areas and habitat features and co-occurring plant species vary significantly between locations. Further, the development of specialized models for detecting specific components of bitou bush, such as flowers only, foliage only, and both together will be important, as will further comparisons between HS data and MS data attained from various sensors. Moreover, there is a need for significantly more training data to strengthen the predictive power of models across varying environments. Since large datasets require significant resources for labelling, efficiencies may be gained in future by employing automatic labelling techniques. By leveraging the diverse datasets acquired by various land managers to improve model accuracy and applicability, it will be possible to identify and further develop the most effective models for bitou bush detection in different environmental settings.

Funding

This project is supported through funding from the Department of Agriculture, Fisheries and Forestry grant round (Grant number: 4-FY9LIKQ), Advancing Pest Animal and Weed Control Solutions, as part of the Established Pest Animal and Weeds Pipeline program.

Ethical statement

Hereby, I Narmilan Amarasingam (Corresponding Author) consciously assure that for the manuscript on "Bitou Bush Detection and Mapping using UAV-based Multispectral and Hyperspectral Imagery and Artificial Intelligence" the following is fulfilled.

1. This material is the authors' own original work, which has not been previously published elsewhere.
2. The paper is not currently being considered for publication elsewhere.
3. The paper properly credits the meaningful contributions of co-authors and co-researchers.
4. All sources used are properly disclosed cited.
5. All authors have been personally and actively involved in substantial work leading to the paper, and will take public responsibility for its content.

I agree with the above statements and declare that this submission follows the policies.

CRediT authorship contribution statement

Narmilan Amarasingam: Conceptualization, Methodology, Visualization, Formal analysis, Writing – original draft. **Jane E Kelly:** Funding acquisition, Project administration, Writing – review & editing. **Juan Sandino:** Writing – review & editing. **Mark Hamilton:** Project administration, Validation, Writing – review & editing. **Felipe Gonzalez:** Supervision, Writing – review & editing. **Remy L Dehaan:** Data curation, Methodology. **Lihong Zheng:** Supervision. **Hillary Cherry:** Funding acquisition, Project administration.

Declaration of competing interest

The authors declare that they have no known competing financial interests or personal relationships that could have appeared to influence the work reported in this paper.

Data availability

Data will be made available on request.

References

Abeysinghe, T., Milas, A.S., Arend, K., Hohman, B., Reil, P., Gregory, A., Vázquez-Ortega, A., 2019. Mapping invasive Phragmites australis in the Old Woman Creek estuary using UAV remote sensing and machine learning classifiers. Rem. Sens. 11 https://doi.org/10.3390/rs11111380.

Ahmed, N., Atzberger, C., Zewdie, W., 2021. Species Distribution Modelling performance and its implication for Sentinel-2-based prediction of invasive Prosopis juliflora in lower Awash River basin, Ethiopia. Ecol. Process 10. https://doi.org/10.1186/s13717-021-00285-6.

Akbari, V., Simpson, M., Maharaj, S., Marino, A., Bhowmik, D., Nagendra Prabhu, G., Rupavatharam, S., Datta, A., Kleczkowski, A., Alice, J., Sujeetha, R.P., 2021. Monitoring Aquatic Weeds in Indian Wetlands Using Multitemporal Remote Sensing Data with Machine Learning Techniques.

Alexandridis, T.K., Tamouridou, A.A., Pantazi, X.E., Lagopodi, A.L., Kashefi, J., Ovakoglou, G., Polychronos, V., Moshou, D., 2017. Novelty detection classifiers in weed mapping: Silybum marianum detection on UAV multispectral images. Sensors (Switzerland) 17. https://doi.org/10.3390/s17092007.

Amarasingam, N., Hamilton, M., Kelly, J.E., Zheng, L., Sandino, J., Gonzalez, F., Dehaan, R.L., Cherry, H., 2023. Autonomous detection of mouse-ear hawkweed using drones, multispectral imagery and supervised machine learning. Rem. Sens. 15 https://doi.org/10.3390/rs15061633.

Chang, A., Yeom, J., Jung, J., Landivar, J., 2020. Comparison of canopy shape and vegetation indices of citrus trees derived from uav multispectral images for characterization of citrus greening disease. Rem. Sens. https://doi.org/10.3390/rs12244122.

Che'ya, N.N., Dunwoody, E., Gupta, M., 2021. Assessment of weed classification using hyperspectral reflectance and optimal multispectral UAV imagery. Agronomy 11. https://doi.org/10.3390/agronomy11071435.

Chikuruwo, C., Masocha, M., Murwira, A., Ndaimani, H., 2017. Predicting the suitable habitat of the invasive Xanthium Strumarium L. In southeastern Zimbabwe. Appl. Ecol. Environ. Res. 15, 17–32. https://doi.org/10.15666/aeer/1501_017032.

Costello, B., Osunkoya, O.O., Sandino, J., Marinic, W., Trotter, P., Shi, B., Gonzalez, F., Dhileepan, K., 2022. Detection of parthenium weed (parthenium hysterophorus L.) and its growth stages using artificial intelligence. Agriculture (Switzerland) 12. https://doi.org/10.3390/agriculture12111838.

da Silva, S.D.P., Eugenio, F.C., Fantinel, R.A., Amaral, L. de P., dos Santos, A.R., Mallmann, C.L., dos Santos, F.D., Pereira, R.S., Ruoso, R., 2023. Modeling and detection of invasive trees using UAV image and machine learning in a subtropical forest in Brazil. Ecol. Inf. 74 https://doi.org/10.1016/j.ecoinf.2023.101989.

de Camargo, T., Schirrmann, M., Landwehr, N., Dammer, K.H., Pflanz, M., 2021. Optimized deep learning model as a basis for fast UAV mapping of weed species in winter wheat crops. Rem. Sens. 13 https://doi.org/10.3390/rs13091704.

Department of Agriculture and Fisheries, 2020. Bitou Bush.

Detka, J., Coyle, H., Gomez, M., Gilbert, G.S., 2023. A drone-powered deep learning methodology for high precision remote sensing in California's coastal shrubs. Drones 7, 421. https://doi.org/10.3390/drones7070421.

Di Gennaro, S.F., Toscano, P., Gatti, M., Poni, S., Berton, A., Matese, A., 2022. Spectral comparison of UAV-based hyper and multispectral cameras for precision viticulture. Rem. Sens. 14 https://doi.org/10.3390/rs14030449.

Dian Bah, M., Hafiane, A., Canals, R., 2018. Deep learning with unsupervised data labeling for weed detection in line crops in UAV images. Rem. Sens. 10 https://doi.org/10.3390/rs10111690.

Ens, E.J., French, K., Bremner, J.B., 2009. Evidence for allelopathy as a mechanism of community composition change by an invasive exotic shrub, Chrysanthemoides monilifera spp. rotundata. Plant Soil 316, 125–137. https://doi.org/10.1007/s11104-008-9765-3.

Etienne, A., Saraswat, D., 2019. Machine Learning Approaches to Automate Weed Detection by UAV Based Sensors. SPIE-Intl Soc Optical Eng, p. 25. https://doi.org/10.1117/12.2520536.

Hamylton, S.M., Morris, R.H., Carvalho, R.C., Roder, N., Barlow, P., Mills, K., Wang, L., 2020. Evaluating techniques for mapping island vegetation from unmanned aerial vehicle (UAV) images: pixel classification, visual interpretation and machine learning approaches. Int. J. Appl. Earth Obs. Geoinf. 89 https://doi.org/10.1016/j.jag.2020.102085.

Haq, M.A., 2021. CNN based automated weed detection system using UAV imagery. Comput. Syst. Sci. Eng. 42, 837–849. https://doi.org/10.32604/csse.2022.023016.

Harris, S., Trotter, P., Gonzalez, F., Sandino, J., 2017. Bitou bush surveillance UAV trial. In: 14th Queensland Weed Symposium.

Harun, M.A.Y. Al, Robinson, R.W., Johnson, J., Uddin, M.N., 2014. Allelopathic potential of Chrysanthemoides monilifera subsp. monilifera (boneseed): a novel weapon in the invasion processes. South Afr. J. Bot. 93, 157–166. https://doi.org/10.1016/j.sajb.2014.04.008.

He, Y., Zhang, X., Zhang, Z., Fang, H., 2022. Automated detection of boundary line in paddy field using MobileV2-UNet and RANSAC. Comput. Electron. Agric. 194 https://doi.org/10.1016/j.compag.2022.106697.

Hu, K., Wang, Z., Coleman, G., Bender, A., Yao, T., Zeng, S., Song, D., Schumann, A., Walsh, M., 2021. Deep Learning Techniques for In-Crop Weed Identification: A Review.

Huang, H., Lan, Y., Deng, J., Yang, A., Deng, X., Zhang, L., Wen, S., 2018. A semantic labeling approach for accurate weed mapping of high resolution UAV imagery. Sensors (Switzerland) 18. https://doi.org/10.3390/s18072113.

Huang, X., Weng, C., Lu, Q., Feng, T., Zhang, L., 2015. Automatic labelling and selection of training samples for high-resolution remote sensing image classification over urban areas. Rem. Sens. 7 (2015), 16024–16044. https://doi.org/10.3390/RS71215819, 7, 16024–16044.

Imran, A.B., Khan, K., Ali, N., Ahmad, N., Ali, A., Shah, K., 2020. Narrow band based and broadband derived vegetation indices using Sentinel-2 Imagery to estimate vegetation biomass. Glob. J. Environ.Sci. Manag. 6, 97–108. https://doi.org/10.22034/gjesm.2020.01.08.

Ishida, T., Kurihara, J., Viray, F.A., Namuco, S.B., Paringit, E.C., Perez, G.J., Takahashi, Y., Marciano, J.J., 2018. A novel approach for vegetation classification using UAV-based hyperspectral imaging. Comput. Electron. Agric. 144, 80–85. https://doi.org/10.1016/j.compag.2017.11.027.

Kerkech, M., Hafiane, A., Canals, R., 2018. Deep leaning approach with colorimetric spaces and vegetation indices for vine diseases detection in UAV images. Comput. Electron. Agric. 155, 237–243. https://doi.org/10.1016/j.compag.2018.10.006.

Khaliq, A., Comba, L., Biglia, A., Ricauda Aimonino, D., Chiaberge, M., Gay, P., 2019. Comparison of satellite and UAV-based multispectral imagery for vineyard variability assessment. Rem. Sens. 11 https://doi.org/10.3390/rs11040436.

Khoshboresh-Masouleh, M., Akhoondzadeh, M., 2021. Improving weed segmentation in sugar beet fields using potentials of multispectral unmanned aerial vehicle images and lightweight deep learning. J. Appl. Remote Sens. 15 https://doi.org/10.1117/1.jrs.15.034510.

Kumar Nagothu, S., Anitha, G., Siranthini, B., Anandi, V., Siva Prasad, P., 2023. Weed detection in agriculture crop using unmanned aerial vehicle and machine learning. Mater. Today Proc. https://doi.org/10.1016/j.matpr.2023.03.350.

Li, Y., Al-Sarayreh, M., Irie, K., Hackell, D., Bourdot, G., Reis, M.M., Ghamkhar, K., 2021. Identification of weeds based on hyperspectral imaging and machine learning. Front. Plant Sci. 11 https://doi.org/10.3389/fpls.2020.611622.

Lindsay, E.A., French, K., 2006. The impact of the weed Chrysanthemoides monilifera ssp. rotundata on coastal leaf litter invertebrates. Biol. Invasions 8, 177–192. https://doi.org/10.1007/s10530-004-5856-0.

Lindsay, E.A., French, K., 2005. Litterfall and nitrogen cycling following invasion by Chrysanthemoides monilifera ssp. rotundata in coastal Australia. J. Appl. Ecol. 42, 556–566. https://doi.org/10.1111/j.1365-2664.2005.01036.x.

Lu, B., He, Y., 2017. Species classification using Unmanned Aerial Vehicle (UAV)-acquired high spatial resolution imagery in a heterogeneous grassland. ISPRS J. Photogrammetry Remote Sens. 128, 73–85. https://doi.org/10.1016/j.isprsjprs.2017.03.011.

Lu, H., Fan, T., Ghimire, P., Deng, L., 2020. Experimental evaluation and consistency comparison of UAV multispectral minisensors. Rem. Sens. 12 https://doi.org/10.3390/RS12162542.

Martín, M.P., Ponce, B., Echavarría, P., Dorado, J., Fernández-Quintanilla, C., 2023. Early-season mapping of johnsongrass (sorghum halepense), common cocklebur (Xanthium strumarium) and velvetleaf (abutilon theophrasti) in corn fields using airborne hyperspectral imagery. Agronomy 13. https://doi.org/10.3390/agronomy13020528.

Narmilan, A., Gonzalez, F., Salgadoe, A.S.A., Kumarasiri, U.W.L.M., Weerasinghe, H.A.S., Kulasekara, B.R., 2022a. Predicting canopy Chlorophyll content in sugarcane crops using machine learning algorithms and spectral vegetation indices derived from UAV multispectral imagery. Rem. Sens. 14, 1140. https://doi.org/10.3390/rs14051140.

Narmilan, A., Gonzalez, F., Salgadoe, A.S.A., Powell, K., 2022b. Detection of white leaf disease in sugarcane using machine learning techniques over UAV multispectral images. Drones 6. https://doi.org/10.3390/drones6090230.

Osorio, K., Puerto, A., Pedraza, C., Jamaica, D., Rodríguez, L., 2020. A deep learning approach for weed detection in lettuce crops using multispectral images. Agric. Eng. 2, 471–488. https://doi.org/10.3390/agriengineering2030032.

Papp, L., van Leeuwen, B., Szilassi, P., Tobak, Z., Szatmári, J., Árvai, M., Mészáros, J., Pásztor, L., 2021. Monitoring invasive plant species using hyperspectral remote sensing data. Land 10, 1–18. https://doi.org/10.3390/land10010029.

Razfar, N., True, J., Bassiouny, R., Venkatesh, V., Kashef, R., 2022. Weed detection in soybean crops using custom lightweight deep learning models. J. Agric. Food Res. 8 https://doi.org/10.1016/j.jafr.2022.100308.

Reedha, R., Dericquebourg, E., Canals, R., Hafiane, A., 2022. Transformer neural network for weed and crop classification of high resolution UAV images. Rem. Sens. 14 https://doi.org/10.3390/rs14030592.

Retallack, A., Finlayson, G., Ostendorf, B., Lewis, M., 2022. Using deep learning to detect an indicator arid shrub in ultra-high-resolution UAV imagery. Ecol. Indicat. 145 https://doi.org/10.1016/j.ecolind.2022.109698.

Roslim, M.H.M., Juraimi, A.S., Che'ya, N.N., Sulaiman, N., Manaf, M.N.H.A., Ramli, Z., Motmainna, M., 2021. Using remote sensing and an unmanned aerial system for weed management in agricultural crops: a review. Agronomy. https://doi.org/10.3390/agronomy11091809.

Sa, I., Popović, M., Khanna, R., Chen, Z., Lottes, P., Liebisch, F., Nieto, J., Stachniss, C., Walter, A., Siegwart, R., 2018. WeedMap: a large-scale semantic weed mapping framework using aerial multispectral imaging and deep neural network for precision farming. Rem. Sens. 10 https://doi.org/10.3390/rs10091423.

Sandino, J., Gonzalez, F., 2018. A novel approach for invasive weeds and vegetation surveys using UAS and artificial intelligence. 2018 23rd international conference on methods and models in automation and robotics. MMAR 2018, 515–520. https://doi.org/10.1109/MMAR.2018.8485874.

Shiferaw, H., Bewket, W., Eckert, S., 2019. Performances of machine learning algorithms for mapping fractional cover of an invasive plant species in a dryland ecosystem. Ecol. Evol. 9, 2562–2574. https://doi.org/10.1002/ece3.4919.

Su, J., Yi, D., Coombes, M., Liu, C., Zhai, X., McDonald-Maier, K., Chen, W.H., 2022. Spectral analysis and mapping of blackgrass weed by leveraging machine learning and UAV multispectral imagery. Comput. Electron. Agric. 192 https://doi.org/10.1016/j.compag.2021.106621.

Vaishnnave, M.P., Srinivasan, P., Suganya Dev, K., ArutPerumJothi, G., 2019. Detection and classification of groundnut leaf diseases using KNN classifier; detection and classification of groundnut leaf diseases using KNN classifier. In: 2019 IEEE International Conference on System, Computation, Automation and Networking (ICSCAN).

Villoslada, M., Bergamo, T.F., Ward, R.D., Burnside, N.G., Joyce, C.B., Bunce, R.G.H., Sepp, K., 2020. Fine scale plant community assessment in coastal meadows using UAV based multispectral data. Ecol. Indicat. 111 https://doi.org/10.1016/j.ecolind.2019.105979.

Wijesingha, J., Dayananda, S., Wachendorf, M., Astor, T., 2021. Comparison of spaceborne and uav-borne remote sensing spectral data for estimating monsoon crop vegetation parameters. Sensors 21. https://doi.org/10.3390/s21082886.

Xia, F., Quan, L., Lou, Z., Sun, D., Li, H., Lv, X., 2022. Identification and comprehensive evaluation of resistant weeds using unmanned aerial vehicle-based multispectral imagery. Front. Plant Sci. 13 https://doi.org/10.3389/fpls.2022.938604.

Yang, C., Everitt, J.H., 2010. Mapping three invasive weeds using airborne hyperspectral imagery. Ecol. Inf. 5, 429–439. https://doi.org/10.1016/j.ecoinf.2010.03.002.

Yu, H., Men, Z., Bi, C., Liu, H., 2022. Research on field soybean weed identification based on an improved UNet model combined with a channel attention mechanism. Front. Plant Sci. 13 https://doi.org/10.3389/fpls.2022.890051.

Yu, R., Luo, Y., Zhou, Q., Zhang, X., Wu, D., Ren, L., 2021. Early detection of pine wilt disease using deep learning algorithms and UAV-based multispectral imagery. Ecol. Manag. 497, 119493 https://doi.org/10.1016/j.foreco.2021.119493.

Zheng, J.Y., Hao, Y.Y., Wang, Y.C., Zhou, S.Q., Wu, W. Ben, Yuan, Q., Gao, Y., Guo, H.Q., Cai, X.X., Zhao, B., 2022. Coastal wetland vegetation classification using pixel-based, object-based and deep learning methods based on RGB-UAV. Land 11. https://doi.org/10.3390/land11112039.